Psilocybin as a Treatment for Repetitive Mild Head Injury: Evidence from Neuroradiology and Molecular Biology

Eric K. Brengel[1,2], Bryce Axe[2], Ashwath Maheswari[2], Muhammad I. Abeer[3], Richard J. Ortiz[4], Taylor J. Woodward[5], Reagan Walhof[5], Rachel Utama[2], Courtney Sawada[2], Shreyas Balaji[2], Praveen P. Kulkarni[1,2], Heather B. Bradshaw[5], Michael A. Gitcho[3], Craig F. Ferris[1,2,6]

[1]Dept Psychology, Northeastern Univ, Boston, MA, USA; [2]Center for Translational Neuroimaging, Northeastern Univ, Boston, MA; [3]Dept Biological Sciences, Delaware State Univ, Dover, DE; [4]Dept Psychology, Northern Illinois Univ, DeKalb, IL; [5]Psychological & Brain Sciences, Program in Neuroscience, Indiana Univ, Bloomington, IN; [6]Dept Pharmaceutical Sciences, Northeastern Univ, Boston, MA

Address all Correspondence to: Craig Ferris, PhD, Director Center for Translational Neuroimaging, 360 Huntington Ave, Boston, Massachusetts, 02115; Email: c.ferris@northeastern.edu; Phone: 508 259 4908

Conflict of Interest: C.F.F. and P.P.K. have a partnership interest in Ekam Imaging Inc., a company that develops RF electronics and 3D MRI atlases for animal research. None of the other authors have a conflict of interest.

Funding: Ekam Imaging Inc. The Paul H. Boerger Fund of the Delaware Community Foundation. Fellowships for M.I.A.: NIH-NIGMS R25GM122722 and National Science Foundation 2023004

Authors' contributions: All contributed equally to the data generation, while E.K.B., B.A., A.M., R.J.O., R.U., and P.P.K. were responsible for MRI and behavior data analysis. H.B.B. and T.J.W. performed blood analysis for lipidomics. M.A.G. and M.I.A. ran studies on molecular biology. E.K.B., P.P.K., H.B.B., M.A.G., and C.F.F. contributed to the concept, experimental design, manuscript preparation, and interpretation.

Acknowledgements: We thank the National Institute on Drug Abuse Drug Supply Program and the Research Triangle Institute for providing the psilocybin used in these studies. We also thank the Center for Translational NeuroImaging and Ekam Imaging for financial support.

Abstract

Repetitive mild head injuries incurred while playing organized sports, during car accidents and falls, or in active military service are a major health problem. These head injuries induce cognitive, motor, and behavioral deficits that can last for months and even years with an increased risk of dementia, Parkinson's disease, and chronic traumatic encephalopathy. There is no approved medical treatment for these types of head injuries. To this end, we tested the healing effects of the psychedelic psilocybin, as it is known to reduce neuroinflammation and enhance neuroplasticity. Using a model of mild repetitive head injury in adult female rats, we provide unprecedented data that psilocybin can reduce vasogenic edema, restore normal vascular reactivity and functional connectivity, reduce phosphorylated tau buildup, enhance levels of brain-derived neurotrophic factor and its receptor TrkB, and modulate lipid signaling molecules.

Introduction

The Centers for Disease Control and Prevention report around 2.9 million people in the United States suffer from traumatic brain injury (TBI) every year, with 70-90% of these categorized as mild TBI[1, 2, 3]. In 2016, the total yearly healthcare expenses for nonfatal TBI exceeded $40.6 billion. This included $10.1 billion from private insurance, $22.5 billion from Medicare, and $8 billion from Medicaid[3]. There is an expanding literature on the behavioral and neurobiological consequences of mild head injuries that are incurred while playing organized sports, during car accidents and falls, or in active military service. Concussion following a single incident is difficult to detect and any associated cognitive and behavioral problems can resolve within hours of insult[4, 5]. However, a more pernicious, long-lasting condition arises when the brain is exposed to repetitive mild traumatic brain injury (rmTBI)[6, 7]. Repetitive head impacts and rmTBI induce cognitive, motor, and behavioral deficits, which are more severe and protracted, and can last for months and even years[8, 9] with an increased risk of dementia, Parkinson's disease[10-14], and chronic traumatic encephalopathy (CTE)[15, 16]. There are no approved treatments for repetitive head impacts, TBI, or rmTBI.

It has been suggested that the serotonergic hallucinogen psilocybin (PSI) could be used to treat brain injury given its known anti-inflammatory effects and its action as a promoter of neuroplasticity and cell growth[17]. A wide range of psychedelics, including PSI, are being evaluated for their potential therapeutic use in various psychiatric disorders[18] including substance abuse[19], severe depression[20, 21], and anxiety[22]. To date, there are no reports of PSI being used to treat any type of head injury. In a recent functional MRI study, we evaluated the dose-dependent effects of PSI on brain activity in fully awake rats. From these studies we determined a 3.0 mg/kg dose of PSI was most effective in stimulating positive blood-oxygen-level-dependent (BOLD) changes in brain activity. In this study, we tested the efficacy of this dose of PSI in a closed-skull momentum exchange model of rmTBI wherein rats were impacted once each day for three consecutive days[23-27]. To make the model more relevant to the human experience, rats were impacted while fully awake and during the dark phase of the light-dark cycle, when they are normally active. There are no mortalities with this model. Absent are any contusions or damage to the skull. Instead, the only gross radiological evidence of head

injury is swelling of the tissue above the skull at the impact site, i.e. a “bump on the head.” A single dose of PSI after each head impact significantly reduced the neuroradiological and molecular measures associated with head injury.

Methods and Materials

Animals

Adult female *(N* = 24) Wistar rats were purchased from Charles River Laboratories (Wilmington, MA, USA). Animals were housed in Plexiglas cages (two per cage) and maintained in ambient temperature (22–24°C). Animals were maintained on a reverse light-dark cycle with lights off at 09:00 and studied during the dark phase when they are normally active. All experiments were conducted between 10:00 and 18:00 to avoid the transitions between the light-dark cycles. Food and water were provided *ad libitum*. Rats were ca. nine months of age when head-impacted and imaged. All animals were acquired and cared for in accordance with the guidelines published in the NIH Guide for the Care and Use of Laboratory Animals. All methods and procedures described below were pre-approved by the Northeastern University Institutional Animal Care and Use Committee under protocol numbers 23-0407R and 24-0517R. Northeastern University’s animal care and use program and housing facilities are fully accredited by AAALAC International. The protocols used in this study followed the ARRIVE guidelines for reporting *in vivo* experiments in animal research[28]. Animals were monitored daily over the duration of the study for general health, including food and water consumption and body weight. A 15% loss in body weight was set as a humane endpoint. Female rats were divided into three experimental groups (*n* = 8; determined by *a priori* power analysis): 1) healthy sham controls injected with saline vehicle but given no head impact (SHAM-VEH), 2) head-impacted and injected with saline vehicle (rmTBI-VEH), and 3) head-impacted and injected with psilocybin (rmTBI-PSI).

Overview

The study began with three consecutive days of mild head injury, psilocybin treatment, and head-twitch response observation. On day three, within an hour of head injury and treatment, blood plasma samples were collected for lipidomic analysis of

103 peripheral biomarkers of mild head injury. This was immediately followed by the first
104 magnetic resonance imaging (MRI) session. Cognitive and motor behaviors were tested
105 on days 4-10. Acclimation for awake neuroimaging occurred on days 15-19 leading up
106 to the second MRI session on day 22. The following day, brain tissue was collected for
107 proteomic analysis. See **Fig 1a** for a timeline of experimental procedures.

108 *Repetitive Mild Head Injury*

109 The momentum exchange model of mild head injury was developed by Viano et
110 al.[29] and further refined by Mychasiuk et al.[30] and Hightower et al.[31] to simulate the
111 dynamics of sport-related concussion in the preclinical setting with fully conscious
112 rodents. Each rat underwent this procedure once per day for three consecutive days.
113 Prior to impact on the first day, all rats were treated with 0.1 mg/kg extended-release
114 buprenorphine analgesic via subcutaneous injection to minimize pain for the duration of
115 the three-day repetitive injury period. Rats were lightly anesthetized via 1-2% isoflurane
116 inhalation to allow for setup in the momentum exchange apparatus. Under anesthesia,
117 rats were secured with a bite bar and strapped to a wheeled cradle sitting atop a
118 chassis to allow for linear and rotational acceleration upon impact. Once fully awake
119 (typically within 1-2 minutes), a pneumatic pressure system is used to reliably propel a
120 50 g impactor toward the head at 7.4 m/s for a kinetic energy input of 1.37 J, simulating
121 the rapid change in head velocity that occurs during concussions in the National
122 Football League[29, 30]. With the head angled downward into the impact plane, all injuries
123 were directed to the approximate area of Bregma. All rats demonstrated normal
124 ambulatory behavior within seconds of being returned to the home cage, and no
125 mortalities, seizures, loss of consciousness, skull fractures, contusions, or other
126 complications were observed. SHAM-VEH control rats underwent all of the above
127 procedures with the exception of head impact; when fully awake, these rats were
128 removed from the apparatus and the impactor was not launched.

129 *Psilocybin administration and Head Twitch Response*

130 Psilocybin was acquired through the National Institute on Drug Abuse (NIDA) and
131 distributed by the Research Triangle Institute. PSI was prepared in sterile saline (0.9%
132 NaCl) at a 3.0 mg/mL concentration for a dose of 3.0 mg/kg via intraperitoneal injection.

Rats were treated within 30 minutes of each head injury (once per day for three days). After each injection, rats were returned to the home cage and recorded from above for 10 minutes for quantification of the head twitch response (HTR), a behavioral indicator of psychoactive dosing. HTR and all subsequent behavioral assays were analyzed without outliers using one-way ANOVA in GraphPad Prism 10.0 software.

Open Field

On day 4, within 24 hours of the last head impact, rats were tested in the Open Field under dim red-light illumination. A detailed description of the Open Field test in rats appears in previous publications[32, 33]. Animals were placed in a lidless black box (60.9 x 69.2 x 70.5 cm) and allowed to explore for 5 minutes while recorded from above. Recordings were processed and data were measured using ANY-maze 7.00 software. In processing, the arena was divided into a peripheral zone (18 cm from the walls) and a central zone (20% of the arena). Agoraphobia (time spent in the center and number of entries to the center), thigmotaxis (time spent along the perimeter), average speed, and total distance traveled were measured and compared.

Novel Object Recognition

On day 5, the Novel Object Recognition task was used to evaluate episodic learning and memory[34-37]. Testing was conducted in the same lidless black box under dim red-light illumination, to which rats were acclimated during Open Field testing the previous day. Rats were first given a 5-minute habituation phase inside the empty box. Rats were then given a 5-minute familiarization phase to explore the box with two identical objects placed in diagonal corners. Lastly, rats returned for the 5-minute test phase, where one familiar object and one new object were presented in the same positions as the familiarization phase. Rats were returned to the home cage to rest for five minutes between each phase. Time spent with the novel and familiar objects during the test phase was measured using ANY-maze 7.00 software and the difference between the two for each subject was analyzed.

Beam Walk

Between days 8-9, rats were trained for motor behavior tasks. A detailed description of the balance beam has been published[36, 38]. We used a tapered balance beam equipped with sensors detecting foot faults across all three segments (wide, middle, thin) to assess fine motor coordination. Animals were acclimated over two days with three training trials per day. During training, they were placed in a goal box for 60 seconds, then on a start platform to cross the beam. Testing occurred over three trials on day 10 with identical conditions. Foot faults and goal box latency were recorded and averaged for each subject.

Rotarod

The Rotarod test is commonly used in Parkinson's disease models to assesses equilibrium and motor function using a 4 cm diameter rotating rod that gradually increases in speed[38]. Animals were acclimated over days 8-9, with three training trials per day. During training, they were placed on the rod rotating at 5 rpm for 3 minutes, and if they fell, they were immediately returned to the rod. Testing occurred over three trials on day 10. The rod started at 1 rpm, accelerating at a rate of 0.2 rpm/s to a maximum of 50 rpm over 245 seconds. The time before animals fell off was recorded and averaged across trials.

Magnetic Resonance Imaging

Imaging was conducted at two timepoints: day 3 (1-2 hours post-injury and treatment) and day 22 (three weeks post-injury and treatment). During the first session, rats were anesthetized with 0.5-1% isoflurane for structural T2-weighted and diffusion weighted imaging (DWI). The entire anesthetized imaging protocol lasted approximately 60 minutes (10 min setup, 6 min T2-weighted MRI, 44 min DWI). For a week before the second session, rats were acclimated for awake imaging. The second session included awake T2-weighted imaging, resting-state functional connectivity (rsFC), and functional MRI with hypercapnic challenge (fMRI), and concluded with anesthetized DWI. The entire imaging protocol lasted approximately 90 minutes, including 45 minutes awake (10 min setup, 6 min T2-weighted MRI, 15 min rsFC, 15 min fMRI) and 45 minutes anesthetized with 0.5-1% isoflurane (DWI).

Imaging sessions were conducted under dim red-light illumination using a Bruker Biospec 7.0 T/20-cm USR horizontal magnet (Bruker, Billerica, MA, USA). Both imaging sessions began with acquisition of a high-resolution T2-weighted anatomical data set using a rapid acquisition, relaxation enhancement (RARE) pulse sequence to screen for motion and to ensure there was no skull fracture or neuroanatomical injury as a result of rmTBI. Due to the length of the imaging procedure, the study was conducted in six staggered cohorts of four rats, with each experimental group randomly distributed across all six cohorts. The animal setup and imaging protocol has been described in detail in previous publications[33, 39-41].

Diffusion Weighted Imaging

DWI was acquired with a 3D spin-echo echo-planar-imaging (3D-EPI) pulse sequence having the following parameters: TR/TE = 500/20 ms, eight EPI segments, and 10 non-collinear gradient directions with a single b-value shell at 1000s/mm^2 and one image with a B-value of 0 s/mm^2 (referred to as B0) as previously described[24, 26, 42]. Geometrical parameters were: 48 coronal slices, each 0.313 mm thick (brain volume) and with in-plane resolution of 0.313 x 0.313 mm^2 (matrix size 96 x 96; FOV 30 mm^3). The imaging protocol was repeated two times for signal averaging. For statistical comparisons among rats, each brain volume was registered to the 3D MRI rat brain atlas for generation of voxel- and region-based statistics. All image transformations and statistical analyses were carried out using the in-house EVA software (Ekam Solutions LLC, Boston, MA, USA). The average value for each region of interest was computed using map files for indices of apparent diffusion coefficient (ADC) and fractional anisotropy (FA). Statistical differences in measures of DWI between experimental groups were determined using a nonparametric Kruskal Wallis multiple comparisons test (critical value set at <0.05) followed by post hoc analyses using a Wilcoxon rank-sum test for individual differences.

Acclimation for awake imaging

To mitigate the stress associated with head restraint, rats were acclimated to the restraining and imaging protocol as previously described[24, 43]. Acclimation sessions were conducted daily for five consecutive days, progressively increasing in duration up

to 45 minutes, the length of the awake imaging setup and acquisition protocol. Respiration, heart rate, motor activity, and plasma corticosterone levels significantly decrease over the course of the acclimation period[44]. This reduction in autonomic and somatic signs of arousal and stress improves signal resolution and image quality.

Resting-State Functional Connectivity

A detailed description of the data acquisition, preprocessing, registration, and analysis has been previously described[33, 41, 45]. Scans were collected using a spin-echo triple-shot EPI sequence with the following parameters: matrix size = 96 x 96 x 20 (H x W x D), TR/TE = 1000/15 ms, voxel size = 0.312 x 0.312 x 1.2mm, slice thickness = 1.2 mm, 200 repetitions, time of acquisition 15 min. Image preprocessing combined AFNI, FSL, DRAMMS, and MATLAB software. After manual skull stripping, data underwent motion correction, outlier removal, slice timing correction, and affine registration to the rat atlas using DRAMMS. Data were then band-pass filtered (0.01-0.1 Hz), detrended, and smoothed (FWHM = 0.8 mm). Nuisance regression removed motion parameters, white matter, and CSF signals. Network analysis was performed in Gephi software using undirected networks from absolute connectivity matrices. Degree centrality was calculated as the sum of connections between each node and all other nodes. Statistical analysis used GraphPad Prism 10.0, with Shapiro-Wilk tests determining normality. Paired t-tests or Wilcoxon signed-rank tests (for non-normal data) compared degree centrality between groups.

Functional MRI with Hypercapnic Challenge

Functional images were captured using a multi-slice Half-Fourier Acquisition Single-Shot Turbo Spin Echo (HASTE) pulse sequence with an in-plane resolution of 312.5 μm^2. The scanning session for CO_2 challenge lasted 15 minutes with 10 acquisitions per minute. Each scanning session was continuous, starting with a 5-minute baseline followed by 5 minutes of 5% CO_2 exposure and 5 minutes after cessation of CO_2.

A detailed description of the data analysis for functional changes in BOLD signal following CO_2 challenge is published[23, 46]. In brief, the fMRI data analysis consisted of three main steps: pre-processing, processing, and post-processing. All these steps were

executed using SPM-12 (available at https://www.fil.ion.ucl.ac.uk/spm/) and in-house MATLAB software. In the pre-processing stage, several operations were performed, including co-registration, motion correction, smoothing, and detrending. In the processing stage, all images were aligned and registered to a 3D Rat Brain Atlas©, which included 173 segmented and annotated brain regions. This alignment was performed using the GUI-based MIVA software developed by Ekam Solutions LLC (Boston, MA, USA). All spatial transformations applied were compiled into a matrix for each subject. Each transformed anatomical pixel location was tagged with its corresponding brain area, resulting in fully segmented representations of individual subjects for localization of functional imaging data to precise 3D volumes of interest.

Each scanning session consisted of 150 data acquisitions. The average signal intensity in each voxel of the first 5 min of baseline (acquisitions 1–50) was compared to 5–10 min (acquisitions 51–100) of CO_2 exposure. We refer to the number of voxels in each brain area that showed a significant increase in BOLD signal above threshold as volume of activation. The mean volume of activation is the average of all rats for each experimental condition for that brain area. Statistical t-tests were performed on each voxel (~ 36,000 voxels in the whole brain) of each subject within their original coordinate system. The baseline threshold was set at 1%. The t-test statistics used a 95% confidence level ($p<0.05$), two-tailed distributions, and heteroscedastic variance assumptions. As a result of the multiple t-test analyses performed, a false-positive detection controlling mechanism was introduced using the formula $P(i) \leq (i/V)(q/c(V))$ across 173 brain areas, where $q=0.2$ and $c(V)=1$.

Lipid Extraction and Partial Purification of plasma

Blood samples were collected 30 minutes after dosing on day 3 via the lateral tail vein. Plasma was isolated via centrifugation and stored in 75μL samples at -80°C until processed as previously described[47, 48]. In brief, methanolic extracts were partially purified using C^{18} solid phase extraction columns (Agilent, Santa Clara, CA, USA). Final elutions (i.e. fractions) of 65, 75, and 100 percent methanol were collected and stored at -80°C until mass spectrometry (MS) analysis.

Lipidomics analysis

280 Methanolic elutions were analyzed as previously described[49] with the exception
281 that the API 7500 (Sciex, Framingham, MA 01701, USA) was used for analysis instead
282 of the API 3000. The API 7500 is coupled to a Shimadzu LC system LC-40DX3 (Kyoto,
283 Japan). Standard curves were generated by using purchased standards (Cayman
284 Chemical, Ann Arbor, MI, USA), and those made in-house were validated through NMR
285 and MS analysis as previously described[50]. Sciex Analyst peak matching software
286 (Sciex, Framingham, MA 01701, USA) was used to validate standard peaks and sample
287 peaks.

288 Statistical analyses for the plasma lipids were completed in IBM SPSS Statistics
289 29 (Chicago, IL, USA). One-way ANOVAs followed by Fisher's Least Significant
290 Analysis of individual endogenous lipids in plasma for each experimental group were
291 analyzed using Student's t-tests set to 2-tails and Type 2. Samples with an endogenous
292 lipid concentration outside of 2 standard deviations from the group mean were omitted
293 from statistics for that compound. Statistical significance for all tests was set at $p < 0.05$,
294 and trending significance at $0.05 < p < 0.10$. Descriptive and inferential statistics were
295 used to create heatmaps for visualizing changes in the concentration of each lipid
296 analyte for every condition as previously described[51].

297 *Molecular biology, Western blot, and solubility fractionation*

298 On day 23, rats were deeply anesthetized via isoflurane inhalation for tissue
299 collection. Brains were rapidly extracted after decapitation, frozen, and stored at -80°C
300 until proteomic analysis. Rat brain samples of frontal area were isolated and solubilized
301 with Douce homogenizer followed by sonification in standard RIPA (50 mM Tris pH 8,
302 150 mM NaCl, 0.5% sodium deoxycholate, 0.1% SDS and 1% NP40) with
303 protease/phosphatase inhibitor as previously described[52]. The solubility fractionation
304 was modified and 200μg total protein from the RIPA-soluble fraction was centrifuged at
305 180,000g for 30 minutes, the supernatant was removed, and the RIPA-insoluble pellet
306 was washed in RIPA buffer and solubilized in 7M urea/2M thiourea before Western blot
307 as previously described[53]. RIPA samples of 20μg each were run on a 4-20% SDS-PAGE
308 and transferred to PVDF, blocked, probed, and visualized as previously described
309 (antibody table)[52].

Statistical analysis for molecular biology

An ANOVA with Tukey post hoc was performed comparing each of the three groups (n = 8 biological replicates/group) reported as mean ± SD. All blots were exposed under the same conditions. All raw uncropped data are available upon request.

Results

Behavior

Shown at the top of **Fig 1a** is a timeline for experimental procedures and data collection. Shown in **Fig 1bc** are the results from the four behavioral assays: Open Field, Beam Walk, Rotarod and Novel Object Recognition. The data collected from each assay is organized into Motor Behavior (top row) and Cognitive and Emotional Behaviors (lower row). The data are shown as dot plots (subjects) and bar graphs (mean ± 95% confidence interval) and analyzed using a one-way ANOVA. HTR was collected each of day 1-3 immediately following PSI or VEH treatment with the other four assays conducted between day 4 and day 10. HTR was observed in all PSI-treated rats exclusively, but only after the first dose and not after subsequent administration on day 2 and day 3. This adaptation has been observed in rodents chronically exposed to hallucinogenic 5-HT2A agonists[54-56]. No significant motor differences were observed across groups for the Beam Walk (time to reach the goal box and number of slips), Rotarod (latency to fall), or Open Field (total distance traveled and average speed). Episodic learning and short-term memory were not significantly different between groups when tested for object recognition. Measures of anxiety associated with fear of open spaces (Agoraphobia) or attachment to protected surfaces (Thigmotaxis) were also not significantly different between experimental groups in the Open Field.

Head Injury and Diffusion Weighted Imaging

Shown in **Fig 2a** are radiograms of each subject for the three experimental groups characterizing the head injury associated with the site of impact near the prefrontal cortex. The areas of impact are characterized by swelling and edema to the soft tissue over the skull, visualized as white contrast in T2-weighted imaging (indicated by arrows). Importantly, no skull fracture or contusion is observed. In three-week follow-

339 up scans, all impact-site edema is resolved. **Fig 2b** reports changes in ADC values
340 collected during DWI 1-2 hours post-injury and treatment on day 3 as a proxy for brain
341 edema. The box insert shows data from the whole brain (173 brain areas). There is a
342 pronounced increase in whole-brain ADC values (paired t-test, $p<0.0001$) comparing
343 SHAM-VEH and rmTBI-VEH rats with a mean difference of 0.06. When comparing all
344 three experimental groups (matched one-way ANOVA), both SHAM-VEH controls and
345 rmTBI-PSI treated rats were significantly less than rmTBI-VEH untreated rats
346 ($p<0.0001$). However, it should be noted that PSI treatment did not reduce all of the
347 edema, as whole-brain measures were still significantly greater than SHAM-VEH. When
348 the 173 brain areas in the rat atlas are organized into brain regions, it is possible to
349 delineate those areas that are more or less sensitive to head injury and PSI treatment
350 as measured by changes in ADC. These data are shown in the bar graphs (mean ± SD)
351 and dot plots (subregions). For example, the hippocampus, comprised of nine brain
352 subregions, showed the same whole-brain profile of ADC values with SHAM-VEH
353 controls and rmTBI-PSI treated rats being less than rmTBI-VEH untreated rats, but with
354 rmTBI-PSI still greater than SHAM-VEH. This is also true for the somatosensory cortex
355 (SS cortex) and the prefrontal cortex. PSI treatment reduced edema to SHAM-VEH
356 levels in the basal ganglia, thalamus, cerebellum, and olfactory system. Specifically, an
357 inverse ADC:FA correlation is detected, indicating whole-brain vasogenic edema. On
358 three-week follow-up scans, all ADC and FA differences were resolved; however, lasting
359 functional changes were detected.

360 *Vascular Reactivity to Hypercapnia*

361 **Fig 3** shows the change in vascular reactivity to carbon dioxide (CO_2) challenge
362 three weeks post-injury and treatment. The box insert shows the number of voxels
363 activated for positive BOLD for the whole brain for each of the experimental conditions.
364 A matched one-way ANOVA shows a significant difference between groups ($F_{(1.583, 267.5)}$
365 $= 90.44$, $p<0.0001$). rmTBI-VEH untreated rats present with significantly higher
366 ($p<0.0001$) voxel numbers than SHAM-VEH controls or rmTBI-PSI treated rats (Tukey's
367 multiple comparison post hoc test), indicating vascular hyperreactivity. The bar graphs
368 (mean ± SD) and dot plots (subregions) show the regional differences in vascular
369 reactivity. In all cases, a matched one-way ANOVA showed a significant difference

370 between groups. Post hoc tests showed that rmTBI-VEH untreated rats were
371 significantly higher than SHAM-VEH controls and, in the case of the basal ganglia,
372 prefrontal cortex, and olfactory system, significantly greater than rmTBI-PSI treated rats.
373 It should be noted rmTBI-PSI treated rats still showed values significantly higher
374 ($p<0.0001$) than SHAM-VEH controls in all brain regions with the exception of the
375 prefrontal cortex, suggesting the treatment was not totally effective in reducing the
376 hyperreactivity to CO_2 challenge following head injury.

377 *Resting-State Functional Connectivity*

378 The bar graphs (mean ± SD) in the highlighted box of **Fig 4a** show the
379 connections to the whole brain for all 173 brain areas three weeks post-injury and
380 treatment. The global statistics using graph theory analysis for the SHAM-VEH controls
381 were Average Degree 14.737, Graph Density 0.087 and Average Path Length 2.541.
382 For rmTBI-VEH untreated rats, the statistics were Average Degree 9.088, Graph
383 Density 0.053, and Average Path Length 2.909. For rmTBI-PSI treated rats, the Average
384 Degree was 35.532, Graph Density 0.209, and Average Path Length 1.892. There was
385 a significant treatment effect using a matched one-way ANOVA [$F_{(1.352,229.8)} = 493.6$,
386 $p<0.0001$)] followed by Tukey's multiple comparison post hoc test (**** $p<0.0001$). The
387 significant differences between each experimental group for different brain regions are
388 shown as dot and bar graphs. The dots represent the different subregions within each
389 brain region.

390 **Fig 4b** shows changes in connectivity to the three midbrain dopaminergic nuclei
391 (ventral tegmental area, substantia nigra compacta, and substantia nigra reticularis).
392 The panels above show the nodes (colored circles) and connections, or edges, (red
393 lines) from the three key dopaminergic nuclei (red circles). This functional connectivity is
394 displayed for all three experimental groups. The differences are dramatic, as rmTBI-
395 VEH untreated rats show an extreme loss of connectivity as compared to SHAM-VEH
396 controls and rmTBI-PSI treated rats. Psilocybin promotes hyperconnectivity, recruiting
397 nodes and connections to and within the thalamus (blue circles) and sensorimotor
398 cortices (yellow circles). The network connections between all nodes (black lines) are
399 shown in the lower panels. rmTBI-VEH untreated rats have very few connections, while

the network connectivity in SHAM-VEH controls, and especially rmTBI-PSI treated rats, is very pronounced. These differences in degrees, or all connections associated with the three dopaminergic nuclei, are shown in the top bar graph (mean ± SD). Both SHAM-VEH controls ($p<0.05$) and rmTBI-PSI treated rats ($p<0.01$) were significantly greater than rmTBI-VEH untreated rats (matched one-way ANOVA, $F_{(1.062, 2.124)} = 32.59$, $p = 0.025$). The difference in degrees associated with the entire dopaminergic system is shown in the bottom bar graph (median, min, and max). Again, SHAM-VEH controls ($p<0.001$) and rmTBI-PSI treated rats ($p<0.0001$) were significantly greater than rmTBI-VEH untreated rats (Kruskal-Wallis test for non-parametric data $p<0.0001$). rmTBI-PSI treated rats were also greater than SHAM-VEH controls ($p<0.0001$), evidence of hyperconnectivity.

Phosphorylated tau reduces to control levels after PSI treatment

The RIPA-soluble protein analysis normalized to tubulin shows a significant increase in phosphorylated tau (PHF-1, provided by Peter Davies) when comparing SHAM-VEH controls to rmTBI-VEH untreated rats ($p = 0.0017$). Interestingly, rmTBI-PSI treated rats show a reduction in phosphorylated tau back to near SHAM-VEH levels ($p = 0.0015$; **Fig 5ab**). The aggregated RIPA-insoluble (urea soluble) phosphorylated tau (PHF-1) shows a significant increase in rmTBI-VEH ($p = 0.0318$) but no change in rmTBI-PSI as compared to SHAM-VEH ($p = 0.2654$; **Fig 5cd**). Though there is no significant decrease in phosphorylated tau aggregation comparing rmTBI-VEH to rmTBI-PSI, there is a distinct clustered trend in reduced aggregated tau and no significant change when SHAM-VEH is compared to rmTBI-PSI ($p = 0.5063$). This lack of urea-soluble aggregation of tau may be due the time of evaluation after injury and future research to examine age-related changes after treatment may show that sustained aggregation may not develop with PSI treatment due to the initial reduction in RIPA-soluble tau. This reduction in aggregation is consistent to what was observed in the RIPA-soluble fraction. However, this significant increase in phosphorylated tau post-injury may be at an early pre-tangle aggregation stage that is reduced to normal levels in PSI-treated animals.

429 In addition, GFAP (astroglia; $p = 0.0378$) and CD11b (microglia; $p = 0.0294$)
430 levels are significantly increased in rmTBI-PSI treated rats relative to SHAM-VEH
431 controls. Changes in gliosis may initially be a protective response to the injury, though it
432 is not significantly different between SHAM-VEH controls and rmTBI-VEH untreated
433 rats[57] (**Fig 5ab**). When astrocyte activation is reduced in an APP/PS1 mouse model,
434 accelerated age-related plaque deposition occurs which implies the need for functional
435 astrocytes to respond to stress[58]. NAD(P)H quinone dehydrogenase 1 (NQO1), induced
436 by the NRF2 antioxidant response pathway (review[59]), has been shown to protect
437 against oxidative stress. rmTBI-PSI treated animals show no significant differences from
438 rmTBI-VEH untreated rats, though there is an associated response increasing NQO1 in
439 rmTBI-VEH ($p = 0.0405$) and rmTBI-PSI ($p = 0.0260$) groups relative to SHAM-VEH
440 (**Fig 5ab**). In rmTBI-PSI treated rats, BDNF shows a significant increase over SHAM-
441 VEH controls ($p = 0.0486$) and a clustered increase over rmTBI-VEH untreated rats ($p =$
442 0.0569). BDNF exerts its effects via the high-affinity tyrosine kinase receptor TrkB[60].
443 Interestingly, TrkB (NTRK2) shows a significant increase in rmTBI-PSI treated rats ($p =$
444 0.0168) compared to SHAM-VEH controls, which may be a protective measure
445 increasing downstream factors (**Fig 5ab**). No significant changes were observed among
446 other RIPA-soluble proteins or urea-soluble phosphorylated TDP-43. These samples
447 were from the frontal area, and the hippocampus and cerebellum may show additional
448 modulations of these pathways. This variability in aggregation may be consistent with
449 the experimental dynamics of our rat rmTBI model consistent with the variability of the
450 human disease. Though phosphorylated TDP-43 in some rats show distinct changes in
451 aggregation, further evaluation of TDP-43, SNCA, amyloid, and other aggregated
452 proteins will be investigated.

453 *Plasma signaling lipids*

454 Two levels of analysis reveal important systemic effects of the intersection of our rmTBI
455 model and repeated PSI treatment. **Fig 6** shows the comparisons of SHAM-VEH versus
456 rmTBI-VEH where the heatmap illustrates the direction of change with rmTBI. Here we
457 see that, overall, there were only three changes in circulating levels of signaling lipids;
458 however, all changes were significant decreases after rmTBI (e.g. stearoyl leucine,

459 stearoyl taurine, and palmitoyl taurine). By contrast, animals treated with PSI who
460 underwent rmTBI had six times as many lipids change as a result of the treatment (3
461 versus 18 respectively), and all significant changes were increases. Key findings were
462 that PSI treatment caused significant increases in most free fatty acids measured and
463 caused reversal of levels of stearoyl taurine, suggesting that this signaling lipid may play
464 a key role in effects of rmTBI.

465 **Discussion**

466 Repetitive mild TBI is very common and can occur over the life span, affecting
467 adolescents playing organized sports, professional athletes, individuals in service, and
468 the elderly. rmTBI is a significant risk factor for dementia, Parkinson's, and
469 Alzheimer's[61]. Neuroinflammation, alterations in gray matter microarchitecture, impaired
470 cerebral blood flow, disruption in blood-brain barrier (BBB) permeability, and dysfunction
471 in clearance of unwanted phosphorylated proteins lie at the heart of these
472 neurodegenerative diseases[62, 63]. The repetitive mild head injury used in this study was
473 designed to reflect the human experience. Our neuroradiological findings recapitulate
474 much of the neuropathology observed and measured in the clinic using MRI. Below, we
475 discuss the "bench to bedside" relevance of these data and the significance of
476 psilocybin as a putative treatment for head injury and neurodegenerative disease.

477 *Model of Repetitive Mild Head Injury*

478 The guidelines from the Centers for Disease Control and Prevention, World
479 Health Organization, and American Congress of Rehabilitation Medicine for diagnosing
480 mild head injuries include self-reports of transient confusion, disorientation, impaired
481 consciousness, or dysfunction in memory around the time of the injury with no
482 neuroradiological evidence of structural damage to the brain[64, 65]. To that end, our lab
483 adopted a head injury model in rats originally developed by Viano and colleagues[29] and
484 further refined by Mychasiuk et al.[30], controlling for the axis of injury, rotational force,
485 and head acceleration in different directions. We have added to this model by
486 performing the mild head impacts while rats are fully awake without the confound of
487 anesthesia and during the active period of their circadian cycle. As was the case in

488 previous studies using this model[23, 66, 67], all rats showed normal ambulatory behavior
489 within seconds of being placed into their home cage after head impact. With this model
490 there are no mortalities and no evidence of skull damage or contusion as determined by
491 MRI. These are the “bump on head, ice pack” injuries that show up on radiograms as
492 edema in the skin at the site of impact as shown in **Fig 2a**. In this model, the
493 neurobiological effects of a single head impact resolve within 24 hours[25]. However, two
494 or more head impacts separated by 24 hours each have long-term consequences, as
495 noted in the clinical literature[68, 69]. In recent publications using this model of rmTBI, our
496 lab has reported a constellation of neurobiological and neurochemical changes in the
497 brains of male and female rats. The pathology includes vasogenic edema[25], altered
498 vascular reactivity[23, 70] and gray matter microstructure[26], disruption in blood-brain barrier
499 permeability[27], reduction in perivascular clearance[24], increases in microgliosis[24, 26],
500 altered astrocytic AQP4 expression and polarization[24], changes in brain functional
501 connectivity[26], and decreased brain-derived neurotrophic factor (BDNF) expression[66]. In
502 the present study we also report elevated levels of phosphorylated tau in the prefrontal
503 cortex of rats weeks after rmTBI.

504 *Mild Repetitive Head Injury and Behavior*

505 Measures of motor activity and coordination and learning and memory were not
506 significantly different across experimental groups. This is not unexpected with mild head
507 impacts in rodents. Anesthetized rats exposed to a single mild head impact[30, 71] or
508 anesthetized mice subjected to five mild head impacts spaced 24 hours apart[72] exhibit
509 minor balance and motor coordination deficits that resolve within a few days. Ren et al.
510 reported that anesthetized mice experiencing a single mild impact show no cognitive
511 changes but do display a decrease in motor performance on the rotarod, lasting up to
512 24 days[73]. In contrast, mice subjected to two mild, repetitive head impacts while fully
513 awake, evaluated through a series of neurobehavioral tests, show complete recovery
514 within hours[74]. Whether the early impacts in our study have long-term effects on
515 behavior as the subjects age remains uncertain. Recurrent mild head injury in humans
516 can lead to persistent post-concussive symptoms that overlap with other psychiatric
517 disorders like PTSD and major depression[75].

518 *Vasogenic Edema*

519 Edema plays a major role in the neuropathology of head injuries[76, 77]. Vasogenic
520 edema results from damage to the BBB, leading to the immediate movement of fluid
521 into the brain's extracellular space. An increase in apparent diffusion coefficient (ADC),
522 which measures water mobility, serves as an indicator of this volume change[77]. This
523 increase in ADC is typically associated with a decrease in fractional anisotropy (FA). In
524 cases of moderate-to-severe head injury, cytotoxic edema occurs, marked by cellular
525 swelling due to disrupted osmolarity regulation across the plasma membrane. This type
526 of edema generally shows a decrease in ADC and an increase in FA[78].

527 In a previous study we found that a single mild impact, which showed no
528 neuroradiological evidence of brain damage, led to a temporary increase in vasogenic
529 edema in the thalamus, basal ganglia, and cerebellum, as indicated by a rise in ADC[25].
530 This increase in extracellular fluid volume peaked at 6 hours and returned to baseline by
531 24 hours. In the present study using three mild head impacts, there was a global
532 increase in ADC values suggestive of vasogenic edema. This increase was shared by
533 several brain regions including the basal ganglia, hippocampus, thalamus, prefrontal
534 cortex, and somatosensory cortex. In each of these cases, treatment with PSI
535 significantly reduced the ADC values. In the basal ganglia and thalamus, these values
536 were reduced to levels measured in SHAM-VEH controls. How does PSI reduce ADC?
537 We would suggest two possible mechanisms: 1) Support BBB structural integrity via
538 endothelial tight junctions to reduce vasogenic edema, and/or 2) enhance astrocytic
539 activity helping to promote convection of excess extracellular fluid through aquaporin
540 channels lining the astrocytic endfeet. With respect to the first, there have been no
541 studies focused solely on PSI and capillary BBB integrity. However, there have been
542 several studies following changes in gene transcription in the cortex in rodents in
543 response to exposure to 5-HT2A psychedelics[79-82]. Most relevant to this study, Jefsen
544 and coworkers showed a significant increase in transcription of select genes in the
545 prefrontal cortex of rats in response to a single dose of PSI [80]. Several of these genes,
546 including Cebpb (CCAAT enhancer binding protein beta); Iκβ-α (NFKBIA), a key

547 regulator of NF-κB signaling; and Nr4a1 (Nur77) are all involved in vascular
548 inflammation and endothelial cell function.

549 In terms of enhanced fluid convention, we have hypothesized in a previous
550 study[83] that astrocytes localized around capillaries form a hydrolytic syncytium
551 connected by gap junctions[84]. Free water from vasogenic edema would move down
552 osmotic gradients, promoting swelling of the astrocytes and hydrostatic pressures
553 favoring convection toward AQP4 water channels at the endfeet surrounding capillaries.
554 PSI causes an elevation in GFAP (Glial Fibrillary Acidic Protein), a filament protein that
555 forms a dynamic intracellular scaffold that interacts with other binding proteins like
556 plectin (cytoskeletal crosslinker) and α-actinin (actin bundling protein) to form a
557 mechanically integrated system that affects astrocytic cell volume[85]. Changes in
558 astrocyte calcium fluctuations enhance phosphorylation and reorganization of the
559 filament structure that could cause mechanical forces, combined with passive osmotic
560 forces, to promote convection, lowering extracellular fluid and decreasing ADC values.

561 *Vascular Reactivity*

562 Fundamental to brain health is autoregulation of cerebral blood flow in the face of
563 fluctuations in systemic blood pressure. At the level of the neurovascular unit,
564 homeostasis is maintained by local changes in vascular reactivity and capillary blood
565 flow in response to the surrounding metabolic environment. A simple biomarker for
566 evaluating the health of cerebral blood vessels is a hypercapnic challenge[86] causing a
567 passive expansion of blood vessels, decreased resistance, and heightened blood flow.
568 Importantly, when exposed to higher levels of CO_2, there is no change in metabolic
569 oxygen consumption. Consequently, the alteration in the MRI signal caused by the
570 increased blood flow in the brain is directly linked to the change in the partial pressure
571 of CO_2. The change in BOLD signal in response to heightened CO_2 levels is a
572 straightforward and reliable technique for evaluating the cerebral vascular reactivity
573 (CVR) in functional imaging studies[87-89]. CO_2-induced changes in BOLD have been
574 used in the clinic to evaluate the health of cerebral vasculature in several neurological
575 disorders including Alzheimer's[90-92], stroke[93], multiple sclerosis[94] and TBI[95]. A recent

576 study by Liu and colleagues evaluated the reliability of hypercapnia-driven CVR as a
577 biomarker for cerebrovascular function and found it was suitable across different
578 scanning platforms and imaging sites for use in longitudinal studies and clinical trials[96].
579 There have been numerous studies using BOLD imaging and hypercapnic
580 challenge to evaluate cerebrovascular function following TBI. With moderate-to-severe
581 TBI there is a significant decrease in CVR in response to CO_2 challenge[95]. Subjects with
582 serious cerebral vascular injury following TBI show reduced global CVR compared to
583 healthy controls[97-99]. Reports of reduced CVR to CO_2 challenge are also true in
584 preclinical studies of TBI[100, 101]. However, there are reports of increased CO_2-induced
585 CVR following mild head injury, [102] particularly in those with sports-related concussions
586 accompanied by reduced CBF and cerebral metabolism[103, 104]. This would suggest
587 enhanced regulation of blood flow to affected areas with reduced metabolism[103, 104]. In
588 this and a previous study on repetitive mild head injury in female rats, [23] we found an
589 increase in CVR with CO_2 challenge. PSI treatment significantly reduced the increase in
590 whole-brain CVR as compared to rmTBI-VEH untreated rats but was still significantly
591 elevated above SHAM-VEH controls. The basal ganglia, prefrontal cortex, and olfactory
592 system were significantly reduced with PSI treatment as compared to rmTBI-VEH
593 untreated rats.

594 *Functional Connectivity*

595 This model of rmTBI presents with global functional hypoconnectivity. This result
596 is not unexpected given the many reports in clinical studies showing a similar decrease
597 in connectivity following head injury. Patients studied within the first seven days of a
598 mild TBI and presenting with post concussive syndrome (PCS) show a reduction in
599 functional connectivity in the sensorimotor and central executive networks as compared
600 to healthy volunteers[105]. Patients with mild TBI and PCS also show decreases in
601 connectivity to the thalamus[106] and a decrease in the symmetry of connectivity between
602 left and right thalamic nuclei[107]. The connectivity between the motor-striatal-thalamic
603 network is also reduced in mild TBI while the frontoparietal network is increased[108].
604 Pinky et al. reported a decrease in functional connectivity in the cerebellum and basal
605 ganglia in sports-related concussions in 12-18-year-olds[109]. Most recently, Fitzgerald

606 and colleagues ran longitudinal studies on young athletes competing in American
607 football, collecting functional connectivity prior to, during, and following the season[110].
608 Patterns of functional connectivity declined during the playing season but recovered
609 after the season ended. They proposed that exposure to multiple head acceleration
610 events may cause changes in brain neurobiology that are similar to concussion but in
611 the absence of any symptomatology. The most robust finding in the present study was
612 the dramatic hyperconnectivity that followed treatment with PSI. Not only did PSI
613 prevent the hypoconnectivity of head injury, it exceeded the normal connectivity of sham
614 controls. This global phenomenon was consistent across multiple brain regions.

615 Given the fact that head injury is one of the major risk factors for the
616 development of Parkinson's disease, we focused on the connectivity of the midbrain
617 dopaminergic system: the ventral tegmental area (VTA) and the substantia nigra (SN)
618 compacta and reticularis. The efferent connections from these brain areas were
619 significantly increased with PSI over rmTBI-VEH untreated rats with a shift toward
620 greater connectivity to the thalamus and somatosensory cortex when compared to
621 SHAM-VEH controls. The dopaminergic system, as defined by the connectivity within
622 and between all these efferent targets from the VTA and SN, was significantly increased
623 over SHAM-VEH and rmTBI-VEH untreated rats.

624 *Psilocybin, BDNF, TrkB, and Phosphorylated Tau*

625 In a recent study using our head injury model, we reported decreased BDNF
626 levels in the hippocampus and around the midbrain dopaminergic nuclei[66]. Both male
627 and female rats 9 months of age show a significant decrease in BDNF in the
628 hippocampus with head injury while males also showed a decrease in BDNF in the
629 substantia nigra. BDNF is the most prevalent neurotrophin in the brain, crucial for the
630 survival, differentiation, synaptic plasticity, and axonal growth of both peripheral and
631 central neurons during adulthood[111]. BDNF exerts its effects via the high-affinity tyrosine
632 kinase receptor TrkB [60]. After spinal cord injury or TBI there is an increase in TrkB
633 mRNA expression at the site of injury[112]. BDNF has been recognized for its significant
634 involvement in cellular processes related to recovery after TBI, such as promoting

635 neuronal survival, axonal growth, and the formation of new synapses[113]. Given its
636 crucial role, BDNF has been extensively studied in experimental TBI models[114]. In a
637 recent study, Moliner et al. reported PSI can directly bind to TrkB receptor with a very
638 high affinity[115]. Further, Zhao et al recently demonstrated the ability of PSI to restore
639 decreases in prefrontal cortex BDNF expression in a rodent model of major depressive
640 disorder[116]. Here, we show that PSI elevated BDNF and TrkB proteins above SHAM-
641 VEH control and rmTBI-VEH untreated rats in the prefrontal cortex. These data provide
642 a possible mechanism of action for the healing effects of PSI.

643 Interestingly, the BDNF/TRK2 pathway is altered in neurodegeneration
644 associated with tauopathies[117], a group of neurodegenerative diseases characterized by
645 the hyperphosphorylation of tau[118]. Tau proteins bind to and stabilize microtubules in
646 neurons to help maintain the structure and function of axons[119]. When tau becomes
647 hyperphosphorylated, it can aggregate into neurofibrillary tangles (NFTs) inside
648 neurons, disrupting cell function[120]. The accumulation of NFTs and the subsequent loss
649 of neuronal function are key features in Alzheimer's disease, frontotemporal dementia,
650 and progressive supranuclear palsy[121-123]. Here, we provide evidence that PSI can
651 reduce phosphorylated tau following head injury, which may ultimately reduce the risk
652 for neurodegenerative diseases.

653 *Plasma lipids as biomarkers of CNS effects*

654 Recently we showed that injections of the endogenous signaling lipid, palmitoyl
655 ethanolamine (PEA) causes significant changes in CNS connectivity and behavior as
656 well as plasma and CNS signaling lipids[33]. These data demonstrate that the presence of
657 signaling lipids in plasma have a direct effect on CNS activity. Data here show that
658 rmTBI alone has a modest but significant effect on signaling lipids by significantly
659 reducing some of the lipids. By contrast, PSI treatment, which significantly improved
660 rmTBI outcomes at multiple levels, drove significant increases in a wide range of
661 circulating signaling lipids. In both cases, these signaling lipids may be key biomarkers
662 for both injury and recovery.

663 The dramatic hyperconnectivity we observed in this study most likely reflects the
664 hyperplastic effects of PSI to enhance synaptogenesis and dendritic growth. Does the

concomitant increase in the blood level of small lipids reflect these morphological changes occurring in neuronal plasma membranes? Indeed, a majority of the brain lipidome composition in the prefrontal cortex of humans, chimpanzees, and macaque monkeys occur prior to adulthood, with significant alterations in lipid concentrations during early development[124]. Lipidomic studies in early childhood have shown marked changes in circulating lipid profiles from birth through early childhood, with specific lipid species showing age-dependent changes[125]. These findings collectively indicate that both postnatal and adolescent periods are characterized by enhanced lipidomic activity in plasma and brain, reflecting critical phases of neurodevelopment and metabolic regulation.

Summary

Repetitive mild head injury affects diverse populations across age groups and is a significant risk factor for neurodegenerative diseases. Our rat model replicates clinical mild TBI by delivering impacts to awake animals during their active phase, producing no structural damage but causing measurable neuropathology. While we observed no significant behavioral deficits—consistent with rapid recovery in mild TBI—our model revealed several key pathological changes.

Diffusion imaging showed widespread increases in ADC values, suggestive of transient vasogenic edema. PSI treatment reduced edema, potentially through two mechanisms: 1) strengthening blood-brain barrier integrity and 2) enhancing astrocytic fluid clearance through GFAP-mediated changes in cell volume regulation.

CO_2 challenge revealed lasting vascular hyperreactivity three weeks after injury, contrasting with the hyporeactivity seen in severe TBI. This suggests compensatory regulation in mild injury. PSI partially normalized this response, particularly in the basal ganglia, prefrontal cortex, and olfactory regions.

Functional connectivity analysis demonstrated global hypoconnectivity post-injury, matching clinical observations in head-injured patients. PSI treatment induced dramatic hyperconnectivity, notably in dopaminergic pathways to thalamic and somatosensory regions. This finding is particularly relevant given the role of rmTBI in risk for Parkinson's disease.

Protein analysis showed an increase in BDNF and TrkB, a possible mechanism of PSI action. BDNF is crucial for neuronal survival and plasticity and acts through TrkB receptors, which increase after brain injury. Recent research shows PSI can directly bind TrkB with high affinity. The ability of PSI to reduce tau phosphorylation suggests potential therapeutic applications beyond rmTBI, possibly extending to other tau-related neurodegenerative disorders.

Modulations in plasma lipids with both rmTBI alone and in conjunction with PSI treatment provide a novel set of biomarkers to exploit for our understanding of how systemic changes in lipid signaling are associated with both long-term damage of rmTBI and the therapeutic effects of psilocybin.

This translational model successfully bridges bench-to-bedside by replicating clinical observations and identifies PSI as a promising therapeutic agent for repetitive mild head injury and its neurodegenerative consequences.

References

1. Peterson, A., Xu, L., Daugherty, J. & Breiding, M. Surveillance Report of Traumatic Brain Injury-Related Emergency Department Visits, Hospitalizations, and Deaths. Centers for Disease Control and Prevention. (2014).
2. Maas, A.I.R.*, et al.* Traumatic brain injury: integrated approaches to improve prevention, clinical care, and research. *Lancet Neurol* **16**, 987-1048 (2017).
3. Centers for Disease Control and Prevention. Economics of Injury and Violence Prevention. (CDC, Atlanta, Georgia, 2024).
4. Lovell, M.R.*, et al.* Recovery from mild concussion in high school athletes. *Journal of neurosurgery* **98**, 296-301 (2003).
5. Pellman, E.J., Lovell, M.R., Viano, D.C. & Casson, I.R. Concussion in professional football: recovery of NFL and high school athletes assessed by computerized neuropsychological testing--Part 12. *Neurosurgery* **58**, 263-274; discussion 263-274 (2006).
6. Guskiewicz, K.M.*, et al.* Cumulative effects associated with recurrent concussion in collegiate football players: the NCAA Concussion Study. *Jama* **290**, 2549-2555 (2003).
7. Marar, M., McIlvain, N.M., Fields, S.K. & Comstock, R.D. Epidemiology of concussions among United States high school athletes in 20 sports. *Am J Sports Med* **40**, 747-755 (2012).
8. De Beaumont, L.*, et al.* Brain function decline in healthy retired athletes who sustained their last sports concussion in early adulthood. *Brain : a journal of neurology* **132**, 695-708 (2009).
9. Gardner, R.C. & Yaffe, K. Epidemiology of mild traumatic brain injury and neurodegenerative disease. *Mol Cell Neurosci* **66**, 75-80 (2015).
10. Crane, P.K.*, et al.* Association of Traumatic Brain Injury With Late-Life Neurodegenerative Conditions and Neuropathologic Findings. *JAMA Neurol* **73**, 1062-1069 (2016).
11. Jafari, S., Etminan, M., Aminzadeh, F. & Samii, A. Head injury and risk of Parkinson disease: a systematic review and meta-analysis. *Movement disorders : official journal of the Movement Disorder Society* **28**, 1222-1229 (2013).

12. Jenkins, P.O., *et al.* Dopaminergic abnormalities following traumatic brain injury. *Brain : a journal of neurology* (2018).

13. Taylor, K.M., *et al.* Head injury at early ages is associated with risk of Parkinson's disease. *Parkinsonism & related disorders* **23**, 57-61 (2016).

14. Gardner, R.C., *et al.* Mild TBI and risk of Parkinson disease: A Chronic Effects of Neurotrauma Consortium Study. *Neurology* **90**, e1771-e1779 (2018).

15. McKee, A.C., *et al.* Chronic traumatic encephalopathy in athletes: progressive tauopathy after repetitive head injury. *Journal of neuropathology and experimental neurology* **68**, 709-735 (2009).

16. Konrad, C., *et al.* Long-term cognitive and emotional consequences of mild traumatic brain injury. *Psychological medicine* **41**, 1197-1211 (2011).

17. Allen, J., Dames, S.S., Foldi, C.J. & Shultz, S.R. Psychedelics for acquired brain injury: a review of molecular mechanisms and therapeutic potential. *Mol Psychiatry* **29**, 671-685 (2024).

18. Banushi, B. & Polito, V. A Comprehensive Review of the Current Status of the Cellular Neurobiology of Psychedelics. *Biology (Basel)* **12** (2023).

19. de Veen, B.T., Schellekens, A.F., Verheij, M.M. & Homberg, J.R. Psilocybin for treating substance use disorders? *Expert Rev Neurother* **17**, 203-212 (2017).

20. Vollenweider, F.X. & Preller, K.H. Psychedelic drugs: neurobiology and potential for treatment of psychiatric disorders. *Nat Rev Neurosci* **21**, 611-624 (2020).

21. Goodwin, G.M., *et al.* Single-Dose Psilocybin for a Treatment-Resistant Episode of Major Depression. *N Engl J Med* **387**, 1637-1648 (2022).

22. Griffiths, R.R., *et al.* Psilocybin produces substantial and sustained decreases in depression and anxiety in patients with life-threatening cancer: A randomized double-blind trial. *J Psychopharmacol* **30**, 1181-1197 (2016).

23. Bens, N., Kulkarni, P. & Ferris, C.F. Changes in cerebral vascular reactivity following mild repetitive head injury in awake rats: modeling the human experience. *Exp Brain Res* **242**, 2433-2442 (2024).

24. Cai, X., *et al.* Mild repetitive head impacts alter perivascular flow in the midbrain dopaminergic system in awake rats. *Brain Commun* **3**, fcab265 (2021).

25. Kulkarni, P.*, et al.* Evidence of early vasogenic edema following minor head impact that can be reduced with a vasopressin V1a receptor antagonist. *Brain Res Bull* **165**, 218-227 (2020).

26. Kulkarni, P.*, et al.* Neuroradiological Changes Following Single or Repetitive Mild TBI. *Front Syst Neurosci* **13**, 34 (2019).

27. Leaston, J.*, et al.* Quantitative Imaging of Blood-Brain Barrier Permeability Following Repetitive Mild Head Impacts. *Front Neurol* **12**, 729464 (2021).

28. Kilkenny, C., Browne, W.J., Cuthill, I.C., Emerson, M. & Altman, D.G. Improving bioscience research reporting: the ARRIVE guidelines for reporting animal research. *PLoS Biol* **8**, e1000412 (2010).

29. Viano, D.C., Hamberger, A., Bolouri, H. & Saljo, A. Concussion in professional football: animal model of brain injury--part 15. *Neurosurgery* **64**, 1162-1173; discussion 1173 (2009).

30. Mychasiuk, R., Hehar, H., Candy, S., Ma, I. & Esser, M.J. The direction of the acceleration and rotational forces associated with mild traumatic brain injury in rodents effect behavioural and molecular outcomes. *J Neurosci Methods* **257**, 168-178 (2016).

31. Hightower R, Brengel E, Prom S, Kulkarni P & 2024;5(3):, F.C. Testing the Efficacy of Minocycline Treatment in an Awake, Female Rat Model of Repetitive Mild Head Injury. *J Exp Neurol.* **5(3)**, 145-161 (2024).

32. Morrison, T.R.*, et al.* Treating head injury using a novel vasopressin 1a receptor antagonist. *Neurosci Lett* **714**, 134565 (2020).

33. Balaji, S.*, et al.* Palmitoylethanolamide causes dose-dependent changes in brain function and the lipidome. *Front Neurosci* **18**, 1506352 (2024).

34. Coleman, J.R.*, et al.* Changes in brain structure and function following chronic exposure to inhaled vaporised cannabis during periadolescence in female and male mice: A multimodal MRI study. *Addict Biol* **27**, e13169 (2022).

35. Demaree, J.L.*, et al.* Exposure to methylphenidate during peri-adolescence decouples the prefrontal cortex: a multimodal MRI study. *Am J Transl Res* **13**, 8480-8495 (2021).

36. Ferris, C.F.*, et al.* Life without a brain: Neuroradiological and behavioral evidence of neuroplasticity necessary to sustain brain function in the face of severe hydrocephalus. *Sci Rep* **9**, 16479 (2019).
37. Harris-Blum, L.*, et al.* Developmental changes in brain structure and function following exposure to oral LSD during adolescence. *Sci Rep* **14**, 18632 (2024).
38. Ferris, C.F.*, et al.* Evidence of Neurobiological Changes in the Presymptomatic PINK1 Knockout Rat. *Journal of Parkinson's disease* **8**, 281-301 (2018).
39. Alkislar, I.*, et al.* Inhaled Cannabis Suppresses Chemotherapy-Induced Neuropathic Nociception by Decoupling the Raphe Nucleus: A Functional Imaging Study in Rats. *Biol Psychiatry Cogn Neurosci Neuroimaging* **6**, 479-489 (2021).
40. Brems, B.M.*, et al.* Dose-dependent effects of GAT107, a novel allosteric agonist-positive allosteric modulator (ago-PAM) for the α7 nicotinic cholinergic receptor: a BOLD phMRI and connectivity study on awake rats. *Front Neurosci* **17**, 1196786 (2023).
41. Ghaw, A.*, et al.* Dose-dependent LSD effects on cortical/thalamic and cerebellar activity: brain oxygen level-dependent fMRI study in awake rats. *Brain Commun* **6**, fcae194 (2024).
42. Ferris, C.F.*, et al.* Alterations in brain neurocircuitry following treatment with the chemotherapeutic agent paclitaxel in rats. *Neurobiology of pain (Cambridge, Mass.)* **6**, 100034 (2019).
43. Cai, X.*, et al.* Imaging the effect of the circadian light-dark cycle on the glymphatic system in awake rats. *Proc Natl Acad Sci U S A* **117**, 668-676 (2020).
44. King, J.A.*, et al.* Procedure for minimizing stress for fMRI studies in conscious rats. *J Neurosci Methods* **148**, 154-160 (2005).
45. Colarusso, B.*, et al.* APOE4 rat model of Alzheimer's disease: sex differences, genetic risk and diet. *BMC Neurosci* **25**, 57 (2024).
46. R, H., E, B., S, P., P, K. & CF, F. Testing the Efficacy of Minocycline Treatment in an Awake, Female Rat Model of Repetitive Mild Head Injury. *Journal Experimental Neurology* **5**, 145-161 (2024).
47. Bradshaw, H.B. & Johnson, C.T. Measuring the Content of Endocannabinoid-Like Compounds in Biological Fluids: A Critical Overview of Sample Preparation Methodologies. *Methods Mol Biol* **2576**, 21-40 (2023).

829 48. Leishman, E., Kunkler, P.E., Hurley, J.H., Miller, S. & Bradshaw, H.B. Bioactive
830 Lipids in Cancer, Inflammation and Related Diseases : Acute and Chronic Mild
831 Traumatic Brain Injury Differentially Changes Levels of Bioactive Lipids in the CNS
832 Associated with Headache. *Adv Exp Med Biol* **1161**, 193-217 (2019).
833 49. Leishman, E., Mackie, K. & Bradshaw, H.B. Elevated Levels of Arachidonic Acid-
834 Derived Lipids Including Prostaglandins and Endocannabinoids Are Present Throughout
835 ABHD12 Knockout Brains: Novel Insights Into the Neurodegenerative Phenotype. *Front*
836 *Mol Neurosci* **12**, 142 (2019).
837 50. Tan, B.*, et al.* Targeted lipidomics: discovery of new fatty acyl amides. *AAPS J* **8**,
838 E461-465 (2006).
839 51. Leishman, E., Mackie, K., Luquet, S. & Bradshaw, H.B. Lipidomics profile of a
840 NAPE-PLD KO mouse provides evidence of a broader role of this enzyme in lipid
841 metabolism in the brain. *Biochim Biophys Acta* **1861**, 491-500 (2016).
842 52. Gitcho, M.A.*, et al.* VCP mutations causing frontotemporal lobar degeneration
843 disrupt localization of TDP-43 and induce cell death. *J Biol Chem* **284**, 12384-12398
844 (2009).
845 53. Neumann, M.*, et al.* Ubiquitinated TDP-43 in frontotemporal lobar degeneration
846 and amyotrophic lateral sclerosis. *Science* **314**, 130-133 (2006).
847 54. Buckholtz, N.S., Zhou, D.F., Freedman, D.X. & Potter, W.Z. Lysergic acid
848 diethylamide (LSD) administration selectively downregulates serotonin2 receptors in rat
849 brain. *Neuropsychopharmacology* **3**, 137-148 (1990).
850 55. Roberts, B.F.*, et al.* Effect of psilocybin on decision-making and motivation in the
851 healthy rat. *Behav Brain Res* **440**, 114262 (2023).
852 56. Smith, D.A., Bailey, J.M., Williams, D. & Fantegrossi, W.E. Tolerance and cross-
853 tolerance to head twitch behavior elicited by phenethylamine- and tryptamine-derived
854 hallucinogens in mice. *J Pharmacol Exp Ther* **351**, 485-491 (2014).
855 57. Shanaki-Bavarsad, M., Almolda, B., Gonzalez, B. & Castellano, B. Astrocyte-
856 targeted Overproduction of IL-10 Reduces Neurodegeneration after TBI. *Exp Neurobiol*
857 **31**, 173-195 (2022).
858 58. Kraft, A.W.*, et al.* Attenuating astrocyte activation accelerates plaque
859 pathogenesis in APP/PS1 mice. *FASEB J* **27**, 187-198 (2013).

860 59. Lu, M.C., Ji, J.A., Jiang, Z.Y. & You, Q.D. The Keap1-Nrf2-ARE Pathway As a
861 Potential Preventive and Therapeutic Target: An Update. *Med Res Rev* **36**, 924-963
862 (2016).
863 60. Klein, R.*, et al.* The trkB tyrosine protein kinase is a receptor for brain-derived
864 neurotrophic factor and neurotrophin-3. *Cell* **66**, 395-403 (1991).
865 61. Spillantini, M.G.*, et al.* Alpha-synuclein in Lewy bodies. *Nature* **388**, 839-840
866 (1997).
867 62. McKee, A.C.*, et al.* The first NINDS/NIBIB consensus meeting to define
868 neuropathological criteria for the diagnosis of chronic traumatic encephalopathy. *Acta*
869 *Neuropathol* **131**, 75-86 (2016).
870 63. Bieniek, K.F.*, et al.* Chronic traumatic encephalopathy pathology in a
871 neurodegenerative disorders brain bank. *Acta Neuropathol* **130**, 877-889 (2015).
872 64. Cassidy, J.D.*, et al.* Incidence, risk factors and prevention of mild traumatic brain
873 injury: results of the WHO Collaborating Centre Task Force on Mild Traumatic Brain
874 Injury. *Journal of rehabilitation medicine*, 28-60 (2004).
875 65. Center for Disease Control and Prevention. National Vital Statistics System,
876 Mortality File. (ed. National Center for Health Statistics) (2015).
877 66. AA, D.S., Kulkarni, P., Ferris, C.F., Amiji, M.M. & Bleier, B.S. Mild repetitive TBI
878 reduces brain-derived neurotrophic factor (BDNF) in the substantia nigra and
879 hippocampus: A preclinical model for testing BDNF-targeted therapeutics. *Exp Neurol*
880 **374**, 114696 (2024).
881 67. R, H., E, B., S, P., P, K. & CF, F. Testing the Efficacy of Minocycline Treatment in
882 an Awake, Female Rat Model of Repetitive Mild Head Injury. *Journal Experimentlal*
883 *Neurology* **5** (2024).
884 68. Gaetz, M., Goodman, D. & Weinberg, H. Electrophysiological evidence for the
885 cumulative effects of concussion. *Brain Inj* **14**, 1077-1088 (2000).
886 69. Iverson, G.L., Gaetz, M., Lovell, M.R. & Collins, M.W. Cumulative effects of
887 concussion in amateur athletes. *Brain Inj* **18**, 433-443 (2004).
888 70. Bens, N., Kulkarni, P. & Ferris, C.F. Changes in cerebral vascular reactivity
889 following mild repetitive head injury in awake rats: modeling the human experience. *Exp*
890 *Brain Res* (2024).

891 71. Christensen, J.*, et al.* When Two Wrongs Make a Right: The Effect of Acute and
892 Chronic Binge Drinking on Traumatic Brain Injury Outcomes in Young Adult Female
893 Rats. *J Neurotrauma* **37**, 273-285 (2020).
894 72. Kane, M.J.*, et al.* A mouse model of human repetitive mild traumatic brain injury.
895 *J Neurosci Methods* **203**, 41-49 (2012).
896 73. Ren, Z.*, et al.* 'Hit & Run' model of closed-skull traumatic brain injury (TBI)
897 reveals complex patterns of post-traumatic AQP4 dysregulation. *J Cereb Blood Flow*
898 *Metab* **33**, 834-845 (2013).
899 74. Tagge, C.A.*, et al.* Concussion, microvascular injury, and early tauopathy in
900 young athletes after impact head injury and an impact concussion mouse model. *Brain :*
901 *a journal of neurology* **141**, 422-458 (2018).
902 75. Howlett, J.R., Nelson, L.D. & Stein, M.B. Mental Health Consequences of
903 Traumatic Brain Injury. *Biol Psychiatry* **91**, 413-420 (2022).
904 76. Katz, D.I., Cohen, S.I. & Alexander, M.P. Mild traumatic brain injury. *Handb Clin*
905 *Neurol* **127**, 131-156 (2015).
906 77. Toth, A. Magnetic Resonance Imaging Application in the Area of Mild and Acute
907 Traumatic Brain Injury: Implications for Diagnostic Markers? in *Brain Neurotrauma:*
908 *Molecular, Neuropsychological, and Rehabilitation Aspects* (ed. F.H. Kobeissy) (Boca
909 Raton (FL), 2015).
910 78. Jha, R.M., Kochanek, P.M. & Simard, J.M. Pathophysiology and treatment of
911 cerebral edema in traumatic brain injury. *Neuropharmacology* **145**, 230-246 (2019).
912 79. Gonzalez-Maeso, J.*, et al.* Hallucinogens recruit specific cortical 5-HT(2A)
913 receptor-mediated signaling pathways to affect behavior. *Neuron* **53**, 439-452 (2007).
914 80. Jefsen, O.H., Elfving, B., Wegener, G. & Muller, H.K. Transcriptional regulation in
915 the rat prefrontal cortex and hippocampus after a single administration of psilocybin. *J*
916 *Psychopharmacol* **35**, 483-493 (2021).
917 81. Martin, D.A., Marona-Lewicka, D., Nichols, D.E. & Nichols, C.D. Chronic LSD
918 alters gene expression profiles in the mPFC relevant to schizophrenia.
919 *Neuropharmacology* **83**, 1-8 (2014).

920 82. Nichols, C.D. & Sanders-Bush, E. A single dose of lysergic acid diethylamide
921 influences gene expression patterns within the mammalian brain.
922 *Neuropsychopharmacology* **26**, 634-642 (2002).
923 83. Ferris, C.F. Rethinking the Conditions and Mechanism for Glymphatic Clearance.
924 *Front Neurosci* **15**, 624690 (2021).
925 84. Giaume, C. & McCarthy, K.D. Control of gap-junctional communication in
926 astrocytic networks. *Trends Neurosci* **19**, 319-325 (1996).
927 85. Ding, M., Eliasson, C., Betsholtz, C., Hamberger, A. & Pekny, M. Altered taurine
928 release following hypotonic stress in astrocytes from mice deficient for GFAP and
929 vimentin. *Brain Res Mol Brain Res* **62**, 77-81 (1998).
930 86. Kassner, A. & Roberts, T.P. Beyond perfusion: cerebral vascular reactivity and
931 assessment of microvascular permeability. *Top Magn Reson Imaging* **15**, 58-65 (2004).
932 87. Davis, T.L., Kwong, K.K., Weisskoff, R.M. & Rosen, B.R. Calibrated functional
933 MRI: mapping the dynamics of oxidative metabolism. *Proc Natl Acad Sci U S A* **95**,
934 1834-1839 (1998).
935 88. Brevard, M.E., Duong, T.Q., King, J.A. & Ferris, C.F. Changes in MRI signal
936 intensity during hypercapnic challenge under conscious and anesthetized conditions.
937 *Magn Reson Imaging* **21**, 995-1001 (2003).
938 89. Sicard, K.M., Henninger, N., Fisher, M., Duong, T.Q. & Ferris, C.F. Long-term
939 changes of functional MRI-based brain function, behavioral status, and histopathology
940 after transient focal cerebral ischemia in rats. *Stroke* **37**, 2593-2600 (2006).
941 90. Sur, S.*, et al.* Association of cerebrovascular reactivity and Alzheimer pathologic
942 markers with cognitive performance. *Neurology* **95**, e962-e972 (2020).
943 91. Glodzik, L., Randall, C., Rusinek, H. & de Leon, M.J. Cerebrovascular reactivity
944 to carbon dioxide in Alzheimer's disease. *J Alzheimers Dis* **35**, 427-440 (2013).
945 92. Yezhuvath, U.S.*, et al.* Forebrain-dominant deficit in cerebrovascular reactivity in
946 Alzheimer's disease. *Neurobiol Aging* **33**, 75-82 (2012).
947 93. Pillai, J.J. & Mikulis, D.J. Cerebrovascular reactivity mapping: an evolving
948 standard for clinical functional imaging. *AJNR Am J Neuroradiol* **36**, 7-13 (2015).
949 94. Pelizzari, L.*, et al.* Cerebrovascular reactivity and its correlation with age in
950 patients with multiple sclerosis. *Brain Imaging Behav* **14**, 1889-1898 (2020).

95. Kenney, K.*, et al.* Cerebral Vascular Injury in Traumatic Brain Injury. *Exp Neurol* **275 Pt 3**, 353-366 (2016).

96. Liu, P.*, et al.* Multi-vendor and multisite evaluation of cerebrovascular reactivity mapping using hypercapnia challenge. *Neuroimage* **245**, 118754 (2021).

97. Amyot, F.*, et al.* Assessment of cerebrovascular dysfunction after traumatic brain injury with fMRI and fNIRS. *Neuroimage Clin* **25**, 102086 (2020).

98. Amyot, F.*, et al.* Imaging of Cerebrovascular Function in Chronic Traumatic Brain Injury. *J Neurotrauma* **35**, 1116-1123 (2018).

99. Haber, M.*, et al.* Vascular Abnormalities within Normal Appearing Tissue in Chronic Traumatic Brain Injury. *J Neurotrauma* **35**, 2250-2258 (2018).

100. Wu, L.*, et al.* Persistent CO(2) reactivity deficits are associated with neurological dysfunction up to one year after repetitive mild closed head injury in adolescent mice. *J Cereb Blood Flow Metab* **41**, 3260-3272 (2021).

101. Golding, E.M.*, et al.* Cerebrovascular reactivity to CO(2) and hypotension after mild cortical impact injury. *Am J Physiol* **277**, H1457-1466 (1999).

102. Mutch, W.A.*, et al.* Longitudinal Brain Magnetic Resonance Imaging CO2 Stress Testing in Individual Adolescent Sports-Related Concussion Patients: A Pilot Study. *Front Neurol* **7**, 107 (2016).

103. Champagne, A.A., Coverdale, N.S., Fernandez-Ruiz, J., Mark, C.I. & Cook, D.J. Compromised resting cerebral metabolism after sport-related concussion: A calibrated MRI study. *Brain Imaging Behav* **15**, 133-146 (2021).

104. Champagne, A.A., Coverdale, N.S., Germuska, M. & Cook, D.J. Multi-parametric analysis reveals metabolic and vascular effects driving differences in BOLD-based cerebrovascular reactivity associated with a history of sport concussion. *Brain Inj* **33**, 1479-1489 (2019).

105. D'Souza, M.M.*, et al.* Alterations of connectivity patterns in functional brain networks in patients with mild traumatic brain injury: A longitudinal resting-state functional magnetic resonance imaging study. *Neuroradiol J* **33**, 186-197 (2020).

106. Messe, A.*, et al.* Specific and evolving resting-state network alterations in post-concussion syndrome following mild traumatic brain injury. *PLoS One* **8**, e65470 (2013).

107. Tang, L.*, et al.* Thalamic resting-state functional networks: disruption in patients with mild traumatic brain injury. *Radiology* **260**, 831-840 (2011).
108. Shumskaya, E., Andriessen, T.M., Norris, D.G. & Vos, P.E. Abnormal whole-brain functional networks in homogeneous acute mild traumatic brain injury. *Neurology* **79**, 175-182 (2012).
109. Pinky, N.N.*, et al.* Multimodal magnetic resonance imaging of youth sport-related concussion reveals acute changes in the cerebellum, basal ganglia, and corpus callosum that resolve with recovery. *Front Hum Neurosci* **16**, 976013 (2022).
110. Fitzgerald, B.*, et al.* Longitudinal changes in resting state fMRI brain self-similarity of asymptomatic high school American football athletes. *Sci Rep* **14**, 1747 (2024).
111. Huang, E.J. & Reichardt, L.F. Neurotrophins: roles in neuronal development and function. *Annu Rev Neurosci* **24**, 677-736 (2001).
112. Zeiler, F.A.*, et al.* Genetic drivers of cerebral blood flow dysfunction in TBI: a speculative synthesis. *Nat Rev Neurol* **15**, 25-39 (2019).
113. Frisen, J.*, et al.* Characterization of glial trkB receptors: differential response to injury in the central and peripheral nervous systems. *Proc Natl Acad Sci U S A* **90**, 4971-4975 (1993).
114. Gustafsson, D., Klang, A., Thams, S. & Rostami, E. The Role of BDNF in Experimental and Clinical Traumatic Brain Injury. *Int J Mol Sci* **22** (2021).
115. Moliner, R.*, et al.* Psychedelics promote plasticity by directly binding to BDNF receptor TrkB. *Nat Neurosci* **26**, 1032-1041 (2023).
116. Zhao, X.*, et al.* Psilocybin promotes neuroplasticity and induces rapid and sustained antidepressant-like effects in mice. *J Psychopharmacol* **38**, 489-499 (2024).
117. Rosa, E.*, et al.* Tau downregulates BDNF expression in animal and cellular models of Alzheimer's disease. *Neurobiol Aging* **48**, 135-142 (2016).
118. Joachim, C.L., Morris, J.H., Selkoe, D.J. & Kosik, K.S. Tau epitopes are incorporated into a range of lesions in Alzheimer's disease. *Journal of neuropathology and experimental neurology* **46**, 611-622 (1987).
119. Weingarten, M.D., Lockwood, A.H., Hwo, S.Y. & Kirschner, M.W. A protein factor essential for microtubule assembly. *Proc Natl Acad Sci U S A* **72**, 1858-1862 (1975).

1012 120. Mandelkow, E.M., *et al.* Tau domains, phosphorylation, and interactions with
1013 microtubules. *Neurobiol Aging* **16**, 355-362; discussion 362-353 (1995).
1014 121. Rippon, G.A., *et al.* Late-onset frontotemporal dementia associated with
1015 progressive supranuclear palsy/argyrophilic grain disease/Alzheimer's disease
1016 pathology. *Neurocase* **11**, 204-211 (2005).
1017 122. Josephs, K.A., *et al.* Neuropathological background of phenotypical variability in
1018 frontotemporal dementia. *Acta Neuropathol* **122**, 137-153 (2011).
1019 123. Dickson, D.W., *et al.* Ballooned neurons in select neurodegenerative diseases
1020 contain phosphorylated neurofilament epitopes. *Acta Neuropathol* **71**, 216-223 (1986).
1021 124. Li, Q., *et al.* Changes in Lipidome Composition during Brain Development in
1022 Humans, Chimpanzees, and Macaque Monkeys. *Mol Biol Evol* **34**, 1155-1166 (2017).
1023 125. Burugupalli, S., *et al.* Ontogeny of circulating lipid metabolism in pregnancy and
1024 early childhood - a longitudinal population study. *Elife* **11** (2022).
1025 126. Stuart, J.M., Paris, J.J., Frye, C. & Bradshaw, H.B. Brain levels of prostaglandins,
1026 endocannabinoids, and related lipids are affected by mating strategies. *Int J Endocrinol*
1027 **2013**, 436252 (2013).

1028

Figure Legends

Fig 1. Experimental Protocol and Behavioral Assessment

a.) Timeline of experimental procedures. **b.**) Motor behavior on the Beam Walk, Rotarod, and Open Field tests. **c.**) Cognitive behavior from Novel Object Recognition and emotional behaviors agoraphobia and thigmotaxis collected from the Open Field test. All behavioral data were collected within one week of the last head impact. One-way ANOVAs showed no significant (ns) differences between any of the experimental groups for any assay.

Fig 2. Diffusion Weighted Imaging: Vasogenic edema reduced by PSI

T2-Weighted Imaging: **a.**) Shown are radiograms of frontal sections of the brain of all subjects taken following the last of three head impacts. The arrows point to the approximate site of impact identified by T2-weighted enhanced signal showing edema on the skin above the skull, but no skull fracture or contusion. This is obvious in all hit rats but not in sham controls. Diffusion Weighted Imaging: **b.**) Shown are whole-brain changes in water diffusivity as measured by apparent diffusion coefficient (ADC) and fractional anisotropy (FA). When comparing SHAM-VEH and rmTBI-VEH there was a global increase in ADC and decrease in FA. There was a significant inverse relationship between ADC and FA values ($r = -.5967$) as shown in the bottom graph. Each red dot is a brain area taken from the rat 3D brain atlas. A comparison across all three experimental groups shows that PSI treatment significantly reduces ADC and increases FA values, reversing the effects of head injury. **c.**) Shown are the regional changes in ADC values for each of the experimental groups. In all brain regions, rmTBI-VEH rats show a significant increase over SHAM-VEH controls, while rmTBI-PSI treated rats show a significant decrease compared to rmTBI-VEH rats. Error bars show standard deviation. * $p<0.05$, ** $p<0.01$, *** $p<0.001$, **** $p<0.0001$

Fig 3. Hypercapnic Challenge: Vascular hyperreactivity reduced by PSI

Shown are changes in vascular reactivity (positive BOLD voxel number) in response to a 5% CO_2 challenge. Whole-brain (box) was significantly elevated above control in rmTBI-VEH rats (gray bars). rmTBI-PSI treated rats were significantly lower than

1059 rmTBI-VEH untreated rats. Regional differences in vascular reactivity are shown in
1060 the bar and dot plots (mean ± SD). Each dot is a subregion in that brain region. *
1061 p<0.05, ** p<0.01, *** p<0.001, **** p<0.0001

1062 **Fig 4. Functional Connectivity: Hypoconnectivity reversed by PSI**

1063 **a.**) Shown are the number of degrees (connections) for the whole brain (red box) for
1064 each experimental group (mean ± SD). Regional differences in degrees are shown in
1065 the bar and dot plots (mean ± SD). Each dot is a subregion of that brain region. In all
1066 cases, rmTBI-PSI treated rats showed greater connectivity than SHAM-VEH or
1067 rmTBI-VEH rats. **b.**) The connectivity to the dopaminergic system for each
1068 experimental condition is shown. The top bar graphs (mean ± SD) to the left show
1069 the number of efferent connections from the three major dopaminergic nuclei in the
1070 midbrain (ventral tegmental area, substantial nigra compacta, and substantia nigra
1071 reticularis) while the radial connectivity maps to the right depict these connections to
1072 color-coded brain regions. The bottom bar graphs to the left (median and 1st and 3rd
1073 quartile) show the number of connections between and within the dopaminergic
1074 system. * p<0.05, ** p<0.01, *** p<0.001, **** p<0.0001

1075 **Fig 5. Proteomics: Phosphorylated tau reduced to control levels by PSI**

1076 **a.**) Western blot of RIPA-soluble proteins. **b.**) Quantitative analysis normalized to
1077 tubulin of RIPA fractions. **c.**) Western blot RIPA insoluble/urea soluble fractions. **d.**)
1078 Quantitative analysis normalized to total protein. Statistical analysis: one way
1079 ANOVA with Tukey post hoc (*n* = 8 biological replicates/3 groups) (e.) * p<0.05 and
1080 ** p<0.002 (all p vales see table).

1081 **Fig 6. Lipidomics: Novel plasma lipid biomarkers modulated by rmTBI and PSI**

1082 The direction of changes for each analysis group relative to SHAM-VEH are
1083 depicted by color and arrow direction, with an increase represented by a green box
1084 and upward arrows and a decrease represented by an orange box with downward
1085 arrows (boxed insert). Level of significance is shown by color shade, wherein
1086 $p < 0.05$ is a dark shade and $0.05 < p < 0.1$ is a light shade. Effect size is represented
1087 by the number of arrows, where 1 arrow corresponds to 1–1.49-fold difference, 2
1088 arrows to a 1.5–1.99-fold difference, 3 arrows to a 2–2.99-fold difference, 4 arrows a

1089 3–9.99-fold difference, and 5 arrows a difference of tenfold or more[126]. An
1090 abbreviation of ‘BDL’ indicates that the lipid concentration that was present in the
1091 sample was below the detectable levels of our equipment while ‘BAL’ indicates
1092 below analytical levels.

1093 **Fig 1. Experimental Protocol and Behavioral Assessment**

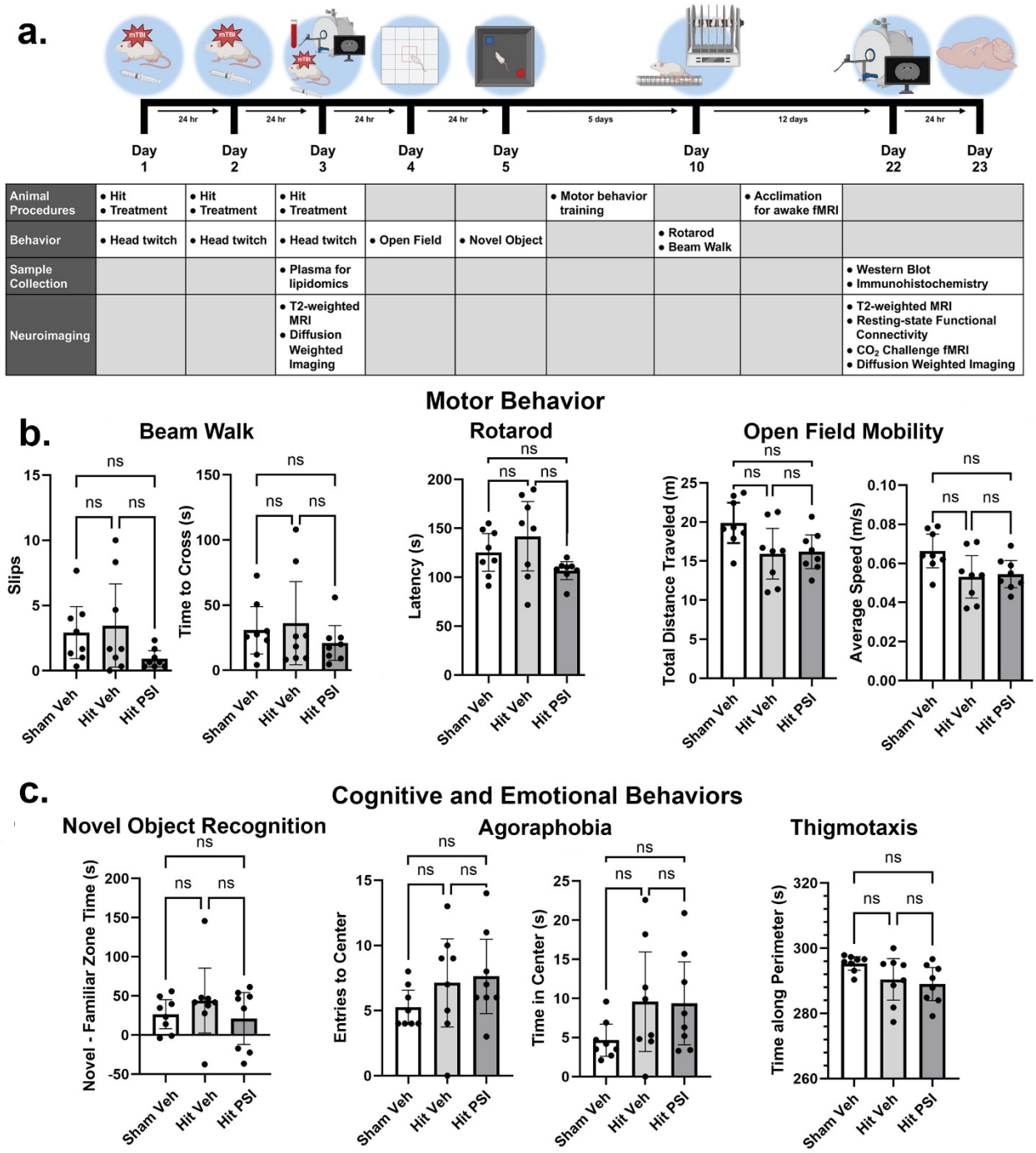

1094

Fig 2. Diffusion Weighted Imaging: Vasogenic edema reduced by PSI

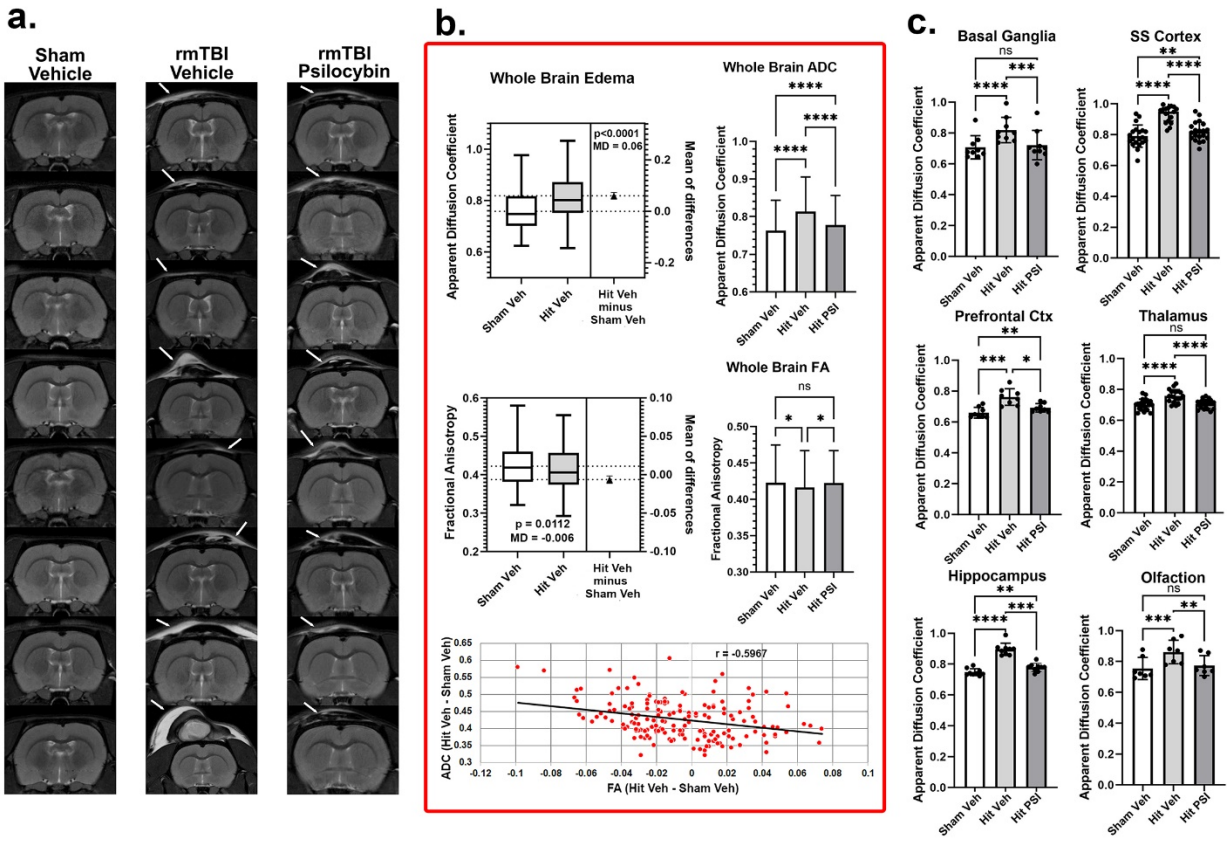

Fig 3. Hypercapnic Challenge: Vascular hyperreactivity reduced by PSI

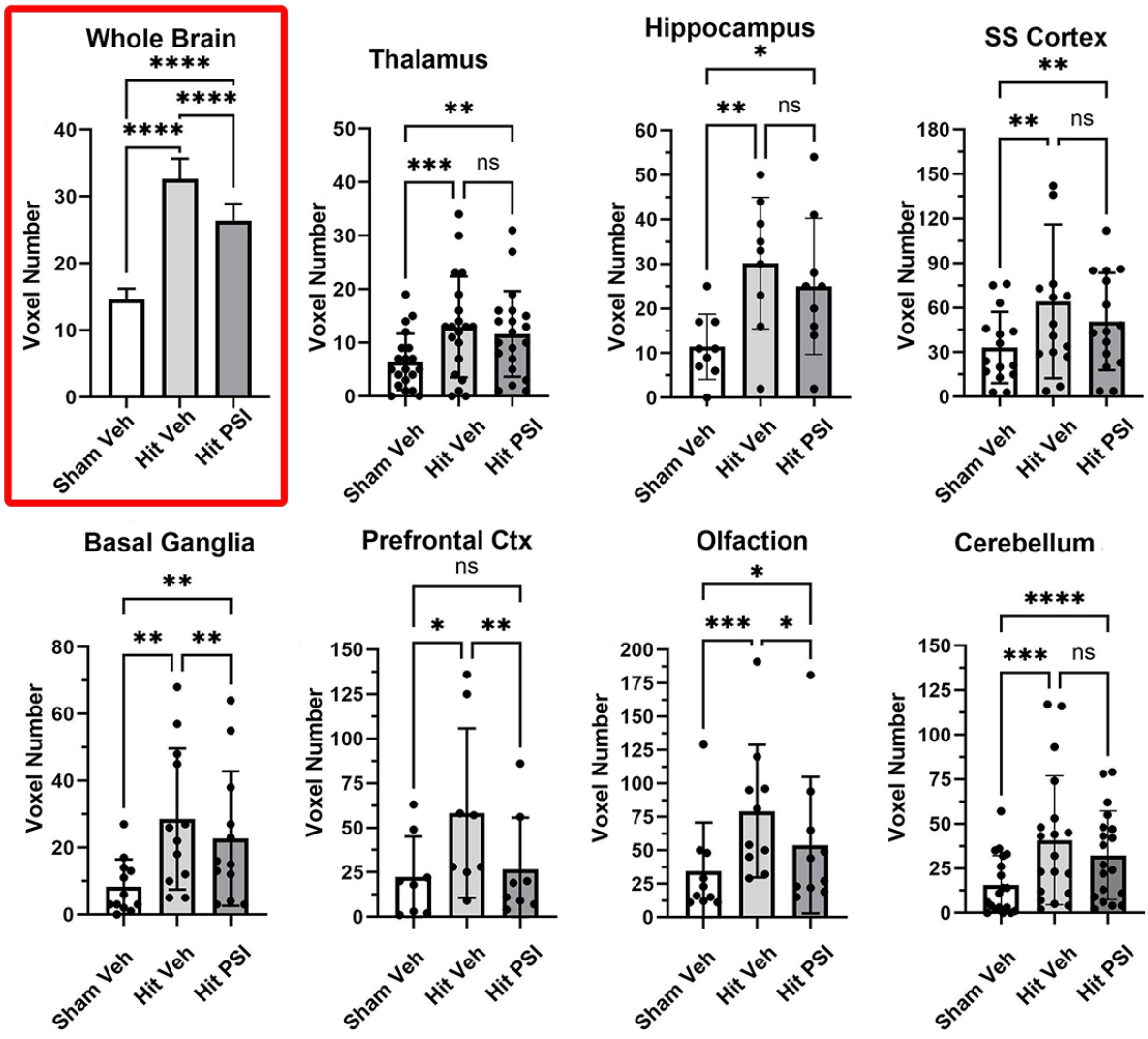

1099 **Fig 4. Functional Connectivity: Hypoconnectivity reversed by PSI**

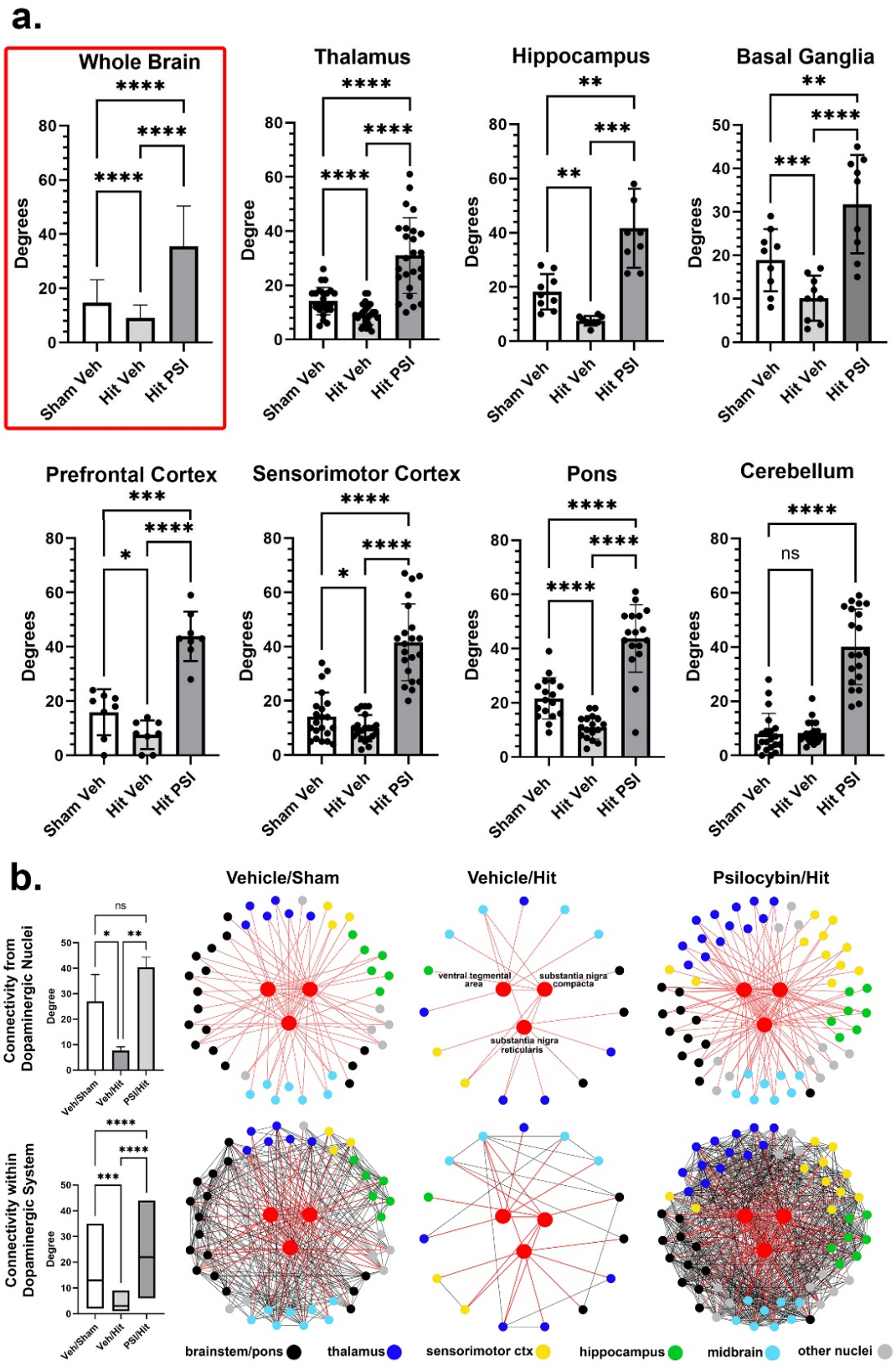

1100 **Fig 5. Proteomics: Phosphorylated tau reduced to control levels by PSI**

1101

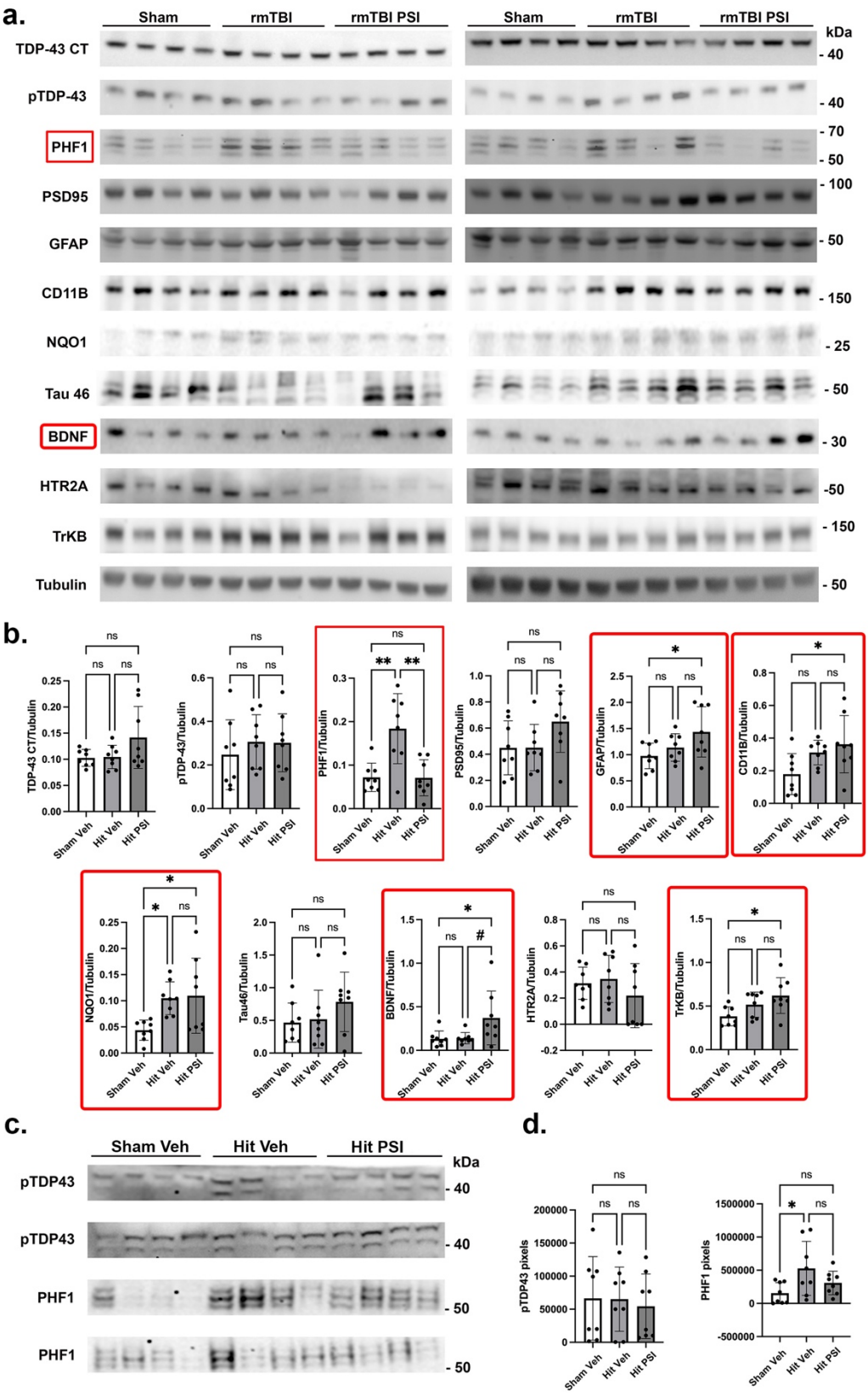

1102 **Fig 6. Lipidomics: Novel plasma lipid biomarkers modulated by rmTBI and PSI**

Small Plasma Lipids	Sham -Vehicle vs Hit -Vehicle	Hit-Vehicle vs Hit-Psilocybin
2-acyl glycerol		
2-palmitoyl glycerol		
2-oleoyl glycerol		
2-linoleoyl glycerol		
2-arachidonoyl glycerol		
N-acyl alanine		
palmitoyl alanine		
stearoyl alanine		
oleoyl alanine		↑↑
linoleoyl alanine		
arachidonoyl alanine	BAL	↑
docosahexaenoyl alanine		
N-acyl ethanolamine		
palmitoyl ethanolamine		
stearoyl ethanolamine		
oleoyl ethanolamine		
linoleoyl ethanolamine		
arachidonoyl ethanolamine		
docosahexaenoyl ethanolamine		
eicosapentaneoyl ethanolamine	BDL	BDL
N-acyl GABA		
palmitoyl GABA	BAL	BAL
stearoyl GABA	BAL	BDL
oleoyl GABA	BDL	BDL
linoleoyl GABA	BDL	BDL
arachidonoyl GABA	BDL	BDL
docosahexaenoyl GABA	BDL	BDL
N-acyl glycine		
palmitoyl glycine		
stearoyl glycine		
oleoyl glycine		↑↑
linoleoyl glycine		↑
arachidonoyl glycine		
docosahexaenoyl glycine		
N-acyl leucine		
palmitoyl leucine		
stearoyl leucine	↓	
oleoyl leucine		
linoleoyl leucine		
arachidonoyl leucine		
docosahexaenoyl leucine		
N-acyl methionine		
palmitoyl methionine		↑
stearoyl methionine		
oleoyl methionine		↑↑
linoleoyl methionine		
docosahexaenoyl methionine		
N-acyl phenylalanine		
palmitoyl phenylalanine		
stearoyl phenylalanine		
oleoyl phenylalanine		
linoleoyl phenylalanine		
arachidonoyl phenylalanine	BAL	BAL
docosahexaenoyl phenylalanine		↑↑
N-acyl proline		
palmitoyl proline		
stearoyl proline		
oleoyl proline	BAL	BAL
linoleoyl proline	BAL	BAL
arachidonoyl proline	BDL	BDL
docosahexaenoyl proline	BDL	BDL

	Sham -Vehicle vs Hit -Vehicle	Hit-Vehicle vs Hit-Psilocybin
N-acyl serine		
palmitoyl serine		
stearoyl serine		
oleoyl serine		↑
linoleoyl serine		↑
arachidonoyl serine	BDL	BDL
docosahexaenoyl serine	BDL	BDL
N-acyl taurine		
palmitoyl taurine	↓	
stearoyl taurine	↓	↑
oleoyl taurine		
arachidonoyl taurine		↑↑
N-acyl tryptophan		
palmitoyl tryptophan	BDL	BDL
stearoyl tryptophan	BDL	BDL
oleoyl tryptophan		
linoleoyl tryptophan	BDL	BDL
arachidonoyl tryptophan	BDL	BDL
docosahexaenoyl tryptophan	BAL	BAL
N-acyl tyrosine		
palmitoyl tyrosine	BAL	BAL
stearoyl tyrosine	BDL	BDL
oleoyl tyrosine		
linoleoyl tyrosine		↑↑
arachidonoyl tyrosine	BDL	BDL
docosahexaenoyl tyrosine	BAL	BAL
N-acyl valine		
palmitoyl valine		
stearoyl valine		
oleoyl valine		
linoleoyl valine		
arachidonoyl valine	BAL	BAL
docosahexaenoyl valine		
Free fatty acids		
oleic acid		↑↑↑
linoleic acid		↑↑↑
arachidonic acid		↑↑
docosahexaenoic acid		↑↑
stearidonic acid		
eicosapentaenoic acid		↑↑

	trending (decrease) (p<0.1-0.51)
	Significant (decrease) (p<0.50)
	Significant (increase) (p<0.50)
	trending (increase) (p<0.1-0.51)
↓	1 - 1.49 times lower
↓↓	1.5 - 1.99 times lower
↓↓↓	2 - 2.99 times lower
↓↓↓↓	3 - 9.99 times lower
↓↓↓↓↓	10 or more times lower
↑	1 - 1.49 times higher
↑↑	1.5 - 1.99 times higher
↑↑↑	2 - 2.99 times higher
↑↑↑↑	3 - 9.99 times higher
↑↑↑↑↑	10 or more times higher